OXFORD UNIVERSITY PRESS | Brain

Microglial activation correlates in vivo with both tau and amyloid in Alzheimer's disease

Journal:	*Brain*
Manuscript ID	BRAIN-2017-01559.R3
Manuscript Type:	Original Article
Date Submitted by the Author:	21-May-2018
Complete List of Authors:	Dani, Melanie; Imperial College London, Neurology Imaging Unit Wood, Melanie; Imperial College London Mizoguchi, Ruth; Imperial College London Fan, Zhen; Imperial College London, Department of Medicine Walker, Zuzana; University College London Medical School, Division of Psychiatry; North Essex Partnership University NHS Foundation Trust, St Margaret's Hospital Morgan, Richard; Chelsea and Westminster Hospital NHS Foundation Trust, Medicine Hinz, Rainer; University of Manchester, Wolfson Molecular Imaging Centre Biju, Maya; 2gether NHS Foundation Trust Kuruvilla, Tarun; 2gether NHS Foundation Trust Brooks, David; Newcastle University; Aarhus Universitetshospital, Department of Nuclear Medicine; Newcastle University, Institute of Neuroscience Edison, Paul; Imperial College London, Neurology Imaging Unit
Subject category:	Dementia
To search keyword list, use whole or part words followed by an *:	Tau imaging < DEMENTIA, Amyloid imaging < DEMENTIA, Microglia < NEURODEGENERATION: CELLULAR AND MOLECULAR, Alzheimer's disease < DEMENTIA, Mild cognitive impairment < DEMENTIA

Microglial activation correlates in vivo with both tau and amyloid in Alzheimer's disease

Running title: Microglial activation, tau and amyloid in Alzheimer's disease

Authors: Melanie Dani[1], Melanie Wood[1], Ruth Mizoguchi[1], Zhen Fan[1], Zuzana Walker[2,3] Richard Morgan[4], Rainer Hinz[5], Maya Biju[6], Tarun Kuruvilla[6], David J Brooks[1,7,8], Paul Edison[1]

Affiliations:

1 Neurology Imaging Unit, Department of Medicine, Imperial College London, UK

2 Division of Psychiatry, University College London, UK

3 Essex Partnership University NHS Foundation Trust

4 Chelsea and Westminster Hospital, London, UK

5 Wolfson Molecular Imaging Centre, University of Manchester, UK

6 [2]Gether NHS Foundation Trust, Rikenel, Montpellier, Gloucester, GL1 1LY, UK

7 Department of Nuclear Medicine, Aarhus University, Denmark

8 Institute of Neuroscience, University of Newcastle upon Tyne, UK

Corresponding author:

Dr Paul Edison MD, MRCP, PhD, FRCP, FRCPI

Neurology Imaging Unit

Division of Brain Sciences

Imperial College London

DuCane Road, Hammersmith Hospital, London, W12 0NN

UK

Tel: +44 203 383 3725

Fax: +00 44 313 4320

Email: paul.edison@imperial.ac.uk

Key words: tau, amyloid, microglia, PET, imaging, Alzheimer, mild cognitive impairment

Abbreviations:

- NIA-AA = National Institute of Ageing and Alzheimer's Association
- NINCDS-ADRDA = National Institute of Neurological and Communicative Disorders and Stroke-AD and Related Disorders Association
- TSPO = translocator protein

Abstract

Alzheimer's disease is characterised by the histopathological presence of β-amyloid plaques and tau containing neurofibrillary tangles. Microglial activation is also a recognised pathological component. The relationship between microglial activation and protein aggregation is still debated. We investigated the relationship between amyloid plaques, tau tangles and activated microglia using PET imaging. Fifty-one subjects (nineteen healthy controls, sixteen mild cognitive impairment (MCI) and sixteen Alzheimer's disease subjects) participated in the study. All subjects had neuropsychometric testing, magnetic resonance imaging (MRI), amyloid (^{18}F-flutemetamol), and microglial (^{11}C-PBR28) PET. All MCI and Alzheimer's disease (AD) subjects and eight of the controls had tau (^{18}F-AV1451) PET. ^{11}C-PBR28 PET was analysed using Logan graphical analysis with an arterial plasma input function, while ^{18}F-flutemetamol and ^{18}F-AV1451 PET were analysed as target: cerebellar ratios to create parametric Standardised Uptake Value Ratio (SUVR) maps. Biological parametric mapping (BPM) in the Statistical Parametric Mapping platform was used to examine correlations between uptake of tracers at a voxel-level.

There were significant widespread clusters of positive correlation between levels of microglial activation and tau aggregation in both the MCI (amyloid positive and amyloid negative) and AD subjects. The correlations were stronger in AD than in MCI, suggesting that these pathologies increase together as disease progresses. Levels of microglial activation and amyloid deposition were also correlated, although in a different spatial distribution; correlations were stronger in MCI than Alzheimer's subjects, in line with a plateauing of amyloid load with disease progression. Clusters of positive correlations between microglial activation and protein aggregation often targeted similar areas of association cortex, indicating that all three processes are present in specific vulnerable brain areas. For the first time using PET imaging, we show that microglial activation can correlate with both tau aggregation and amyloid deposition. This confirms the complex relationship between these processes. These results suggest that preventative treatment for Alzheimer's disease should target all three processes.

Introduction

Despite extensive research in recent decades, no cure has been identified for Alzheimer's disease, and the precise mechanisms of the underlying pathologies are still unclear. Cardinal pathological features are amyloid β (Aβ) plaques and neurofibrillary tangles composed of hyperphosphorylated tau (Perl, 2010; Serrano-Pozo *et al.*, 2011a). A third feature, which is also important in the disease process, is microglial activation. Microglial cells are the intrinsic macrophages of the central nervous system and are responsible for monitoring and responding to injury and insult in the surrounding brain (Pasqualetti *et al.*, 2015). Activated microglial cells surround abnormally aggregated protein and are thought to represent the brain's natural defence mechanism as they attempt to clear the protein fibrils. In Alzheimer's disease and other neurodegenerative diseases, microglial activation becomes persistent and eventually ineffective (Heneka *et al.*, 2015; Pasqualetti *et al.*, 2015). In addition, the products of microglia chronically activated by aggregated Aβ (pro-inflammatory cytokines such as Tumour Necrosis Factor α, Interleukin-6, Interleukin-1α, Granulocyte Macrophage-Colony Stimulating Factor) can cause toxic damage to surrounding cells, the severity of which increases as disease progresses (Serrano-Pozo *et al.*, 2016)(Serrano-Pozo *et al.*, 2016)(Serrano-Pozo *et al.*, 2016). Histopathological studies have shown that activated microglial cells surround amyloid plaques (Perlmutter, 1990; Stalder *et al.*, 1999) and neurofibrillary tangles (Sheffield, 2000; Serrano-Pozo *et al.*, 2011b), possibly in an attempt to clear them. However, other studies suggest that microglial activation may be an early process in disease pathogenesis, causing abnormal protein aggregation (Yoshiyama *et al.*, 2007; Lee *et al.*, 2015). The precise role of microglial activation and in particular its relationship to amyloid deposition and tau aggregation is still debated.

Given that amyloid deposition plateaus around the time of onset of symptoms (Villemagne *et al.*, 2013) and that in established disease persistent microglial activation may lead to neuronal damage and tau aggregation (Sheffield, 2000), we hypothesised that levels of microglial activation would correlate with neurofibrillary tangle load in established Alzheimer's disease, while in mild cognitive impairment, microglial activation would correlate with amyloid deposition.

Positron Emission Tomography (PET) imaging allows us to detect and quantify microglial activation, amyloid deposition and tau aggregation in vivo, and provides spatial information about the extent of these molecular processes - information that was only previously available

at end stage post-mortem. Additionally, advanced image processing and quantification using Biological Parametric Mapping (Casanova *et al.*, 2007) allows us to interrogate the inter-relationship between these processes at a voxel level. ^{18}F-flutemetamol PET is a marker of fibrillar amyloid β (Ikonomovic *et al.*, 2016) while ^{18}F-AV1451 PET is a high affinity marker of paired helical filament-tau (Xia *et al.*, 2013). ^{11}C-PBR28 PET is a marker of translocator protein which is expressed by the outer mitochondrial membrane of the activated microglia associated with Alzheimer's disease (Kreisl *et al.*, 2013).

The aim of this study was to evaluate in vivo the spatial inter-relationship between microglial activation, tau aggregation, and amyloid deposition in mild cognitive impairment and Alzheimer's disease subjects.

Materials and Methods

Study population

This study was approved by national and local ethics committees - the Riverside Research Ethics Committee, National Health Research Services, Health Research Authority, UK. Approval for administration of PET tracers was obtained from the Administration of Radioactive Substances Advisory Committee (ARSAC). Written informed consent was obtained from all subjects.

Recruitment

Subjects were recruited from local memory clinics, a national dementia recruitment website and advertisements in local media. After providing informed consent, subjects underwent a screening visit, and their clinical diagnosis of mild cognitive impairment and Alzheimer's disease was confirmed after checking the clinical and neurological findings, MRI scans and neuropsychometric evaluation. The Petersen criteria (Petersen *et al.*, 2004) were used for the diagnosis of mild cognitive impairment subjects, while NIA-AA (National Institute of Ageing and Alzheimer's Association)(McKhann *et al.*, 2011) or NINCDS-ADRDA (National Institute of Neurological and Communicative Disorders and Stroke-AD and Related Disorders Association criteria (McKhann *et al.*, 1984) were used for the diagnosis of Alzheimer's disease. Subjects were then stratified according to whether they carried one or two copies of the Ala147Thr polymorphism of the TSPO gene as high affinity binders, mixed

affinity binders, or low affinity binders of ^{11}C-PBR28 (Owen *et al.*, 2012). Low affinity binders were excluded from the study.

Inclusion criteria were: 1) A diagnosis of mild cognitive impairment according to the Petersen criteria, or Alzheimer's disease fulfilling NINCDS-ADRDA or NIA-AA criteria, or normal cognition for the healthy controls. 2) Age range 50-85 years. 3) Ability to give informed consent. 4) At least 8 years of formal education. 5) Mini-Mental Examination State score above 24 for mild cognitive impairment, above 15 for Alzheimer's disease, and normal cognition for healthy controls. Exclusion criteria were: 1) History of major depression, or any significant disease influencing neuropsychological testing. 2) Schizophrenia or schizoaffective disorder. 3) Inability to undergo MRI scanning. 4) A malignancy within the last 5 years (except localised skin or prostate cancer).

In total, fifty-one subjects (nineteen healthy controls, sixteen mild cognitive impairment and sixteen clinical Alzheimer's disease subjects participated in the study. Along with neuropsychometric testing and MRI scanning, all subjects had ^{18}F-flutemetamol PET, and eighteen of the nineteen had ^{11}C-PBR28 PET. All mild cognitive impairment and Alzheimer's disease subjects and seven of the controls had ^{18}F-AV1451 PET.

Image acquisition

MRI

Subjects had Magnetic Resonance Imaging (MRI) with a 3 Tesla Siemens Verio scanner and a 32-channel head coil. A T1-weighted magnetisation prepared rapid gradient echo sequence (MPRAGE; time repetition = 2400 ms, time echo = 3.06 ms, flip angle of 9, inversion time = 900 ms, matrix = [256 x 246]) with a 1mm^3 voxel size, anteroposterior phase encoding direction, and a symmetric echo was employed. Two subjects with coronary artery stents (who were therefore ineligible for 3 Tesla MRI) underwent 1.5 Tesla MRI with a Philips Achieva system (Best, Netherlands) at the MRC Clinical Sciences Centre, Imperial College London.

PET imaging

^{11}C-PBR28

^{11}C-PBR28 was manufactured at the Imanova Centre for Imaging Sciences in London and imaging was performed at the same centre with a Siemens Truepoint PET/CT (axial field of view of 21.8cm; 111 transaxial planes; spatial resolution of 2.056mm x 2.056 mm x 2 mm after image reconstruction). A mean dose of 330.9 (±30) MBq of ^{11}C-PBR28 in 20ml normal saline was injected. Dynamic data was acquired in 3D and list mode over 90 minutes and the data was rebinned using the following time frames; 8x15 seconds, 3x60 seconds, 5x120 seconds, 5x300 seconds, 5x600 seconds. Arterial blood was sampled (via a radial artery cannula) continuously with an online detector for the first 15 minutes and discrete blood samples were taken at 5, 10, 20, 30, 50, 70 and 90 minutes. Samples were centrifuged to measure whole blood and plasma radioactivity along with radioactive metabolite levels. Reverse-phase chromatography was used to analyse plasma metabolites. Data reconstruction was performed by filtered back projection, (2.6 zoom, and 5mm Gaussian filter).

^{18}F-flutemetamol

^{18}F-flutemetamol was made by GE Healthcare, Amersham, UK. Scans were performed at Imperial College Clinical Imaging Facility using a Siemens Biograph 6 scanner with a 15cm field of view. A mean dose of 183.4 (±5.3) MBq of ^{18}F-Flutemetamol was injected in 8ml saline followed by a 10ml saline flush. Data was acquired in 3D list mode from 90 to 120 minutes following injection (6x5 minute frames). Image reconstruction was performed by filtered back projection with attenuation correction. Post reconstruction 5mm Gaussian smoothing was performed. The zoom was 2.6, the matrix size was 168x168 and the pixel size was 1.56mm x 1.56mm x 1.92mm.

^{18}F-AV1451

^{18}F-AV1451 was manufactured at Imanova Centre for Imaging Sciences, London, and scans were acquired using the same Siemens Truepoint PET/CT scanner as for ^{11}C-PBR28 PET. A mean dose of 168.3 (±7.4) MBq ^{18}F-AV1451 was injected in 20 ml saline. Data was acquired in 3D list mode for 120 minutes (frames of 8x15 seconds, 3x 60 seconds, 5x120 seconds, 5x300 seconds, 8x600 seconds). Data reconstruction was performed with iterative reconstruction and 5mm Gaussian smoothing was applied post reconstruction.

Image processing

MRI and PET scans were pre-processed using Analyze AVW 11.0. Image processing was performed in Analyze AVW 11.0 and Statistical Parametric Mapping 5 (SPM5, Wellcome

Trust Centre for Neuroimaging, University College London) on a Matlab platform. Voxel level correlations were interrogated using the Biological Parametric Mapping toolbox, which is integrated into Statistical Parametric Mapping software. ^{11}C-PBR28 parametric V_T images were created with in-house MICK.exe parametric mapping software "MICK (Modelling, Input functions and Compartmental Kinetics) version 5.2 software (available on request from Wolfson Molecular Imaging Centre, University of Manchester, Manchester, UK (Dr Rainer Hinz)) was used to fit all regional compartmental models with the Nelder-Mead optimisation algorithm (Nelder and Mead, 1965). MICK uses MATLAB R2009bSP1 (The MathWorks, Natick, MA, USA)(Fan *et al.*, 2016; McGinnity *et al.*, 2017).

^{11}C-PBR28 processing

Logan graphical analysis was used to create parametric maps of V_T at a voxel level using metabolite corrected arterial plasma input functions and dynamic PET time activity curves (TACs) for each subject. MICK software was used to generate a parametric map of ^{11}C-PBR28 V_T from the slope of the Logan plot (Logan, 2000). The V_T map was then co-registered to the T1-weighted volumetric MRI scan, and transformed into Montreal Neurologic Institute standard space.

^{18}F-Flutemetamol and ^{18}F-AV1451

The 90-120 minute summed ^{18}F-Flutemetamol and 80-100 minute summed ^{18}F-AV1451 PET images were co-registered to their T1-weighted MRI, and transformed into Montreal Neurological Institute space. The individual's MRI was segmented into grey matter, white matter and cerebrospinal fluid (CSF) using Analyze AVW. Grey matter voxels were defined has having >50% probability of being grey matter and Analyze AVW was used to create individualised grey matter binary images. The binarised image was then convolved with the Hammers probabilistic atlas (Hammers, 2003) to create an individualised object map. The cerebellum was then sampled, and target-to-cerebellar uptake ratio images were produced by dividing the summed image by the uptake of cerebellar grey matter uptake in Analyze AVW. Region of interest analysis was performed by sampling these ratio images using individualised object maps.

PET images were analysed both with and without a partial volume correction for reduction due to any atrophy present in the MRIs of mild cognitive impairment and Alzheimer disease

subjects. Partial volume correction was performed by structural-functional synergy for resolution recovery (SFS-RR) on a Matlab platform. (Shidahara et al., 2009)

Voxel-level group comparisons

Normalised co-registered PET images (target:cerebellar ratio images for ^{18}F-AV1451 and ^{18}F-flutemetamol and Logan V_T parametric maps for ^{11}C-PBR28) for each disease group were compared to the controls using an independent t-test in SPM. A p value of <0.05 was considered significant, and no voxel extent threshold was used. For ^{11}C-PBR28 PET, each group was compared to the respective control group according to binding status.

Additionally, to identify whether each individual was 'positive' for tracer binding, a single-subject comparison was performed in SPM as an independent t-test compared to the mean of the respective control group.

Determining amyloid status

Based on region of interest analysis of their SUVR ^{18}F-Flutemetamol images, subjects were classified as amyloid positive or negative. Subjects were classified as amyloid positive if they had increased binding (compared to control mean + 2 standard deviations) in one or more cortical regions (frontal, parietal, temporal, occipital lobe, anterior cingulate and posterior cingulate cortex). This was confirmed on visual read. Subjects were deemed positive for tau tangles and microglial activation if they had increased tracer binding (relative to control mean + 2 standard deviations) in the left or right hippocampus, parahippocampus, amygdala, fusiform gyrus, temporal lobe, frontal lobe, parietal lobe, or occipital lobe.

Generation of Z-score maps and voxel-level correlations using biological parametric mapping analysis

The biological parametric mapping toolbox (Casanova et al., 2007) was used to create Z-score maps of tracer uptake for each subject. Generating tracer Z-maps for each subject allows spatial correlations between the uptake of the different tracers with different means and variances to be interrogated and reveals the inter-relationships of each Alzheimer pathology.

The Z-score maps were created in SPM5 using the following formulae:

Z score (^{11}C-PBR28 V_T) = (^{11}C-PBR28 Logan V_T of individual – Mean of the control ^{11}C-PBR28 Logan V_T)/Standard deviation of ^{11}C-PBR28 control Logan V_T

Z score (^{18}F-flutemetamol) = Individual ^{18}F-flutemetamol ratio image - control mean of ^{18}F-flutemetamol ratio/standard deviation of control ^{18}F-flutemetamol

Z-score (^{18}F-AV1451) = individual ^{18}F-AV1451 ratio – control mean of ^{18}F-AV1451 ratio/standard deviation of control ^{18}F-AV1451

For ^{11}C-PBR28 images, Z-maps were generated from the appropriate control cohort according to the TSPO binding status of each subject. ^{11}C-PBR28 uptake of mild cognitive impairment and Alzheimer's disease cases who were high or mixed affinity binders was compared with mean uptake of the high or mixed affinity binders in the control group. After Z-maps were generated (so accounting for effects of binding status), the medium and high affinity binders were then combined for analysis as one group.

The voxel-level correlations between microglial activation, amyloid load, and tau aggregation were interrogated across individual Z-score maps using the Biological Parametric Mapping toolbox for all groups. To assess significance of correlations between ^{18}F-Flutemetamol and ^{11}C-PBR28 uptake, and ^{18}F-AV1451 and ^{11}C-PBR28 uptake in the amyloid negative subjects, a statistical threshold was set at $p<0.05$ with an extent threshold of 500 voxels. Given the highly significant positive correlations between ^{18}F-AV1451 and ^{11}C-PBR28 in the amyloid positive mild cognitive impairment and Alzheimer's disease groups, we set the cluster level of significance at 0.01, and the extent threshold at 500 voxels for these correlation analyses. All clusters with a corrected p-value of $p<0.05$ were considered significant. P-values were corrected for family-wise errors.

Results

Demographics

All nineteen healthy controls in our fifty-one subjects scanned were amyloid negative. Nine mild cognitive impairment subjects were amyloid positive while seven were negative. Of the sixteen subjects with a clinical diagnosis of Alzheimer's disease, fourteen were amyloid positive and two were negative. These two subjects had a clinical diagnosis of probable Alzheimer's disease based on the NINCDS-ADRDA criteria, but had negative amyloid PET scans. Both individuals had impaired neuropsychometric tests in multiple domains that affected activities of daily life. The MRIs of both subjects showed reduced hippocampal volume. Their diagnoses had been made in a hospital clinic settings, and was reconfirmed on the initial screening visit.

Table 1 shows the demographic and neuropsychometric details of the cohort. As expected, neuropsychometric tests revealed impaired scores for both mild cognitive impairment and Alzheimer's disease subjects. The mean delay between ^{18}F-flutemetamol and ^{11}C-PBR scans was 2.1 months; and ^{18}F-AV1451 and ^{11}C-PBR28 scans was 8 months. The amyloid positive MCI subjects were significantly older than the amyloid negative subjects, with significantly worse delayed visual recall, delayed word list recall and semantic fluency.

Voxel-level group differences

Figure 1 shows the voxel-level distribution of increased ^{18}F-flutemetamol, ^{18}F-AV1451 and ^{11}C-PBR28 uptake (only the high affinity binders are shown for ^{11}C-PBR28 as these represented the majority of these cases – eight of the Alzheimer's disease cases, four of the mild cognitive impairment cases and seven of the amyloid negative cases compared to the control group).

Although the clusters show trends for increased uptake, there were no significantly increased clusters in the Alzheimer's disease or amyloid negative group compared to the controls at a group level.

However, when we examined tracer uptake for each individual compared to the control group, distinct binding patterns emerged. In the Alzheimer's disease group (all of whom were amyloid positive), five had increased tau and microglial activation; nine only had increased

tau. In the amyloid positive mild cognitive impairment group, four had increased tau, while two had increased microglial activation and one had both increased tau and microglial activation. In the amyloid negative group, three individuals had increased tau and microglial activation, two had increased microglial activation and one had increased tau only. Clusters of each individual's increase binding for ^{11}C-PBR and ^{18}F-AV1451 are shown in Supplementary table 4. There were six individuals (five Alzheimer's disease and one amyloid positive MCI) who had increased binding of all three tracers.

In order to visually display the spatial distributions of tracer binding, the mean summed images are shown for each group and each tracer in Supplementary Figure 1. Data for the eighteen healthy control subjects who had ^{11}C-PBR28 PET (eleven high affinity binders and seven mixed affinity binders) are shown in Supplementary figure 4).

Voxel-level correlations

There were clusters of highly significant positive correlations throughout the cortex between microglial activation and both tau aggregation and amyloid deposition in the Alzheimer's disease and mild cognitive impairment subjects (shown in Figures 2 and 3). There were extensive clusters of positive correlations, with a larger area of involvement and higher Z-scores, between microglial activation and tau aggregation compared with microglial activation and amyloid deposition. There were also clusters of positive correlations between microglial activation and tau aggregation in the amyloid negative group throughout the isocortex. (Figure 2)

Tau and microglial activation (Amyloid positive individuals)

Positive correlations between ^{18}F-AV1451 and ^{11}C-PBR28 uptake are shown in Supplementary Table 1. In the mild cognitive impairment group, there were positive correlations in the frontal, temporal, parietal and cingulate but not the occipital cortices. The strongest correlations in the group, with the highest Z-scores and correlation coefficients, were in the frontal lobe.

In the Alzheimer's disease group, there were significant positive correlations between ^{18}F-AV1451 and ^{11}C-PBR28 uptake in the frontal, temporal, parietal, occipital, and insular cortices. The strongest correlations were seen in the frontal and temporal lobes and the Z-scores were higher in the Alzheimer's disease compared to the MCI group, indicating increasing tau-inflammation correlations at voxel level as the disease advances.

The clusters of positive correlations in the temporal lobe differed between the mild cognitive impairment and Alzheimer's disease groups: the mild cognitive impairment group had positive clusters in the posterior temporal lobes and left fusiform gyrus while the distribution was more diffuse in the Alzheimer's disease group – the anterior, posterior, lateral (fusiform gyrus) and medial temporal (amygdala and hippocampus) lobes all had clusters of significant correlation (Table 2).

Examples of correlation plots from individual single voxels within clusters are shown in Supplementary Figure 3. Correlation plots from the voxels with the highest Z-scores and correlation coefficients have been illustrated.

Amyloid negative individuals

There were two individuals with a clinical diagnosis of Alzheimer's disease who were amyloid negative. The results for these subjects were combined with the amyloid negative mild cognitive impairment individuals when performing the Biological Parametric Mapping correlation analysis, as they were likely to represent non-Alzheimer syndromes. Individual voxel level increases of tau aggregation and microglial activation for the nine individuals are shown in Figure 5. Positive correlations are shown in Supplementary Table 1.

Tau aggregation and microglial activation were positively correlated in this group, with clusters in the right superior parietal gyrus, left posterior temporal lobe, left lateral part of occipital lobe and right superior frontal gyrus. The areas of positive correlation were smaller with lower Z-scores and lower correlation coefficients than those seen for the amyloid positive groups.

Amyloid and microglial activation (Amyloid positive individuals)

There were positive correlations throughout the cortex in both Alzheimer's disease and mild cognitive impairment subjects. However, MCI subjects showed more extensive regions of correlation with higher correlation coefficients and Z-scores compared to the Alzheimer's disease group. The most widespread distribution of positive correlations in the mild cognitive impairment group was in the frontal and temporal cortex, while in the Alzheimer's disease group, the parietal cortex had the widest distribution of clusters. The locations of regions of positive correlations are shown in Supplementary Table 1 and Figure 3.

Regions where microglial activation correlated with both tau aggregation and amyloid deposition

Certain regions had clusters of positive correlations between microglial activation and both amyloid deposition and tau aggregation across all the groups (mild cognitive impairment and Alzheimer's disease, amyloid positive and negative). These regions included the posterior temporal lobe and superior frontal gyrus. Other regions that were commonly affected in more than one group were the lateral part of the occipital lobe and inferolateral part of the parietal lobe.

Tracer positive individuals only

Next, to ensure that our correlations were not false positives arising from inclusion of 'null data points' from tracer negative individuals, and to address the fact that there were not significant differences between the AD group and controls, we analysed the six individuals (one mild cognitive impairment and five Alzheimer's disease individuals) who were positive at voxel level for binding of all three tracers. As the number of these subjects was small, they were analysed as a single group. Correlations are shown in Supplementary Table 2a, and group differences with controls for each tracer are shown in Supplementary Table 2b. Individual levels of microglial activation correlated strongly with levels of both amyloid deposition and tau aggregation across the cortex, with Z-scores above 4 (Figure 4). The clusters with the strongest correlations between amyloid and microglial activation were localised in the precentral, inferior and middle frontal gyri. The strongest correlations between tau and microglial activation were localised in the superior, middle and inferior frontal gyri.

The clusters of positive correlations between tau and microglial activation were of a similar size, correlation strength and distribution in this small sub-group.

Partial volume correction of images

Clusters of correlated uptake across the tracers using partial volume corrected images are shown in Supplementary Table 3 and Supplementary Figure 2. Interestingly, when partial volume correction was applied, the correlations became more widespread and showed higher Z-scores and r-correlation coefficients than the non-partial volume corrected images. The pattern of positive correlations, and the stronger correlation between microglial activation and tau aggregation in Alzheimer's disease than mild cognitive impairment persisted.

Discussion

In this first reported PET study to examine microglial activation, tau aggregation and amyloid deposition in subjects with mild cognitive impairment and Alzheimer's disease, we found clusters where microglial activation is strongly correlated at a voxel level with both tau aggregation and amyloid deposition. There were also significant positive correlations between tau aggregation and microglial activation in our amyloid-negative cognitively impaired group.

Correlations between tau aggregation and microglial activation were stronger in the Alzheimer's disease group compared to the mild cognitive impairment group, with higher Z-scores, higher correlation coefficients (r) and a wider distribution of clusters, particularly in the temporal lobe where tau aggregation is known to increase in intensity through the Braak stages (Braak and Braak, 1991). These findings support previous histopathological and in vitro studies, which have shown that microglial activation parallels tau aggregation as disease progresses (Sheffield, 2000; Serrano-Pozo et al., 2011b). In addition, microglial activation correlates with the spread of tau aggregation in the brain (Maphis et al., 2015b). The pro-inflammatory products of microglial activation promote tau hyperphosphorylation in vitro (Quintanilla et al., 2004; Gorlovoy et al., 2009; Lee et al., 2010; Maphis et al., 2015b), which in turn induces tau neurofibrillary tangle formation; this may then cause further microglial activation, (Zilka et al., 2009) resulting in a positive feedback cycle as disease progresses (Figure 6). This could apply to our mild cognitive impairment/Alzheimer's disease cohort, however, longitudinal studies are needed to provide more insight into mechanisms driving progression of disease rather than a cross-sectional study.

Clusters of correlations between amyloid and microglial activation were predominantly localised in the isocortex – that is the frontal, temporal, parietal and occipital, insular and anterior cingulate cortices. These findings support previous histopathological findings that have described microglia surrounding cortical amyloid plaques (Perlmutter, 1990; Stalder et al., 1999). Interestingly, the area of distribution was wider and the strength of correlations was higher in the mild cognitive impairment subjects compared to the Alzheimer's disease group. This may be because amyloid deposition occurs early in the disease process triggering microglial activation in an attempt to clear the plaques. A peak of early microglial activation could occur when amyloid deposition first takes place a decade before symptoms appear (Villemagne et al., 2013) followed by a decline in microglial activation as amyloid load

plateaus followed by a second peak as neurofibrillary tangles form and intensify across the cortex (Serrano-Pozo et al., 2011b).

The fact that tau aggregation and microglial activation were correlated in our amyloid negative individuals (albeit less strongly than in the amyloid positive individuals) suggests that amyloid is not necessary for a cycle of tau tangle – activated microglia – tau tangle feedback. Microglial activation may drive tauopathies playing a similar underlying pathogenic role to that in Alzheimer's disease – that is, promoting tau hyperphosphorylation and propagation in the brain. This is in line with previous in vivo findings of increased microglial activation in tauopathies (Paulus et al., 1993; Ishizawa and Dickson, 2001; ishizawa et al., 2004). The consistent pattern of inflammation seen in cognitively impaired tau positive individuals who were positive and negative for amyloid, suggests that the findings are not due to false positives.

Two amyloid negative dementia subjects had a clinical diagnosis of Alzheimer's disease based on NINCDS-ADRDA criteria, and cognitive impairment in multiple domains, affecting activities of daily life. Both had evidence of elevated ^{18}F-AV1451 binding in the temporal lobe substructures (on sampling of the ratio image), and both had elevated ^{11}C-PBR28 V_T calculated from a two tissue compartment model (data not shown). While these individuals are unlikely to have Alzheimer's disease (according to their biomarker profile), they represent a significant proportion of Alzheimer's disease 'mimics'. Clinical trials and autopsy studies show that 15%-16% of individuals with a diagnosis of 'probable Alzheimer's disease' have insufficient neuropathological changes to confirm the diagnosis (Salloway et al., 2014; Serrano-Pozo et al., 2014). Notably, when examining the distributions of tau aggregation and microglial activation in each of the nine individuals, the distributions and patterns of each tracer differed, emphasising the heterogeneity of pathologies in these individuals.). This group was small, with only three individuals demonstrating increased binding of both ^{11}C-PBR28 and ^{18}F-AV1451, and there were no group mean differences from the controls in either pathology. However, five individual subjects had increased microglial activation and four had increased tau aggregation compared with the controls, emphasising the heterogeneity of pathologies in these individuals. One possible diagnosis could be Primary Age-related Tauopathy (PART) where isolated neurofibrillary tangles are localised to the medial temporal lobe, across a spectrum of cognitive ability (Crary et al., 2014), although microglial activation has not been reported in this condition. Microglial activation can play a role in other neurodegenerative diseases such as dementia with Lewy bodies, frontotemporal

dementia and Parkinson's disease (Cagnin et al., 2004; Surendranathan et al., 2015). Additionally, mixed pathologies in the ageing brain are very common (Schneider et al., 2009) and the relationship between microglial activation and other senile pathologies such as TDP43 aggregation, hippocampal sclerosis and argyrophilic grain disease are still unknown. Finally, small vessel disease can be associated with microglial activation which is a well-recognised subacute response to stroke (Vidale et al., 2017; Zhao et al., 2017) and occurs after cerebral hypoperfusion in mice (Manso et al., 2017). Thus, the presence of microglial activation in both patients with and without amyloid may be related to independent processes altogether, with tau hyperphosphorylation representing the end of a final common pathway.

Although this study was not longitudinal so inferences about temporal changes in the disease process cannot be made, it is interesting that amyloid load correlated with inflammation levels most strongly in mild cognitive impairment whereas tau load correlated most strongly with inflammation levels in Alzheimer's disease by which time amyloid plaque load has plateaued but tau tangles are still increasing. In vitro studies suggest that microglial activation may actually cause up-regulation of both tau and amyloid pathology (Lee et al., 2015), again supporting the positive feedback mechanism, and explaining the rapid progression of cortical neurofibrillary tangles in Alzheimer's disease. Furthermore, tau protein in a pathological form may actually be required for microglia-induced cell toxicity, showing again the complex inter-play between the pathologies (Maphis et al., 2015a). While the clusters of positive correlations are indicative of the relative timing of pathologies – that is that peaks of microglial activation occur as first amyloid and then tau aggregation increases in the cortex - the exact temporal and spatial patterns of disease cannot be inferred from this cross sectional data and a longitudinal follow up study is required.

While our data shed some light on the relative distributions and correlations of microglial activation in mild cognitive impairment and Alzheimer's disease, the relationship between amyloid plaques, tau tangles and microglial activation is clearly complex. Recent reports suggest that cortical amyloid plaque deposition is required to promote isocortical, though not subcortical, tau aggregation in a synergistic manner so driving disease progression (Pascoal et al., 2016). Recent biomarker studies (Pontecorvo et al., 2017) and older histopathological work (Price and Morris, 1999) show that amyloid deposition and tau aggregation start independently of each other (amyloid in the isocortical areas, tau neurofibrillary tangles in the medial temporal lobe), but that the spread of tau to the isocortical areas is dependent on the presence of amyloid fibrils. The spatial dissociation of this synergism is unexplained, but

may be due to amyloid cross-seeding tau along functional networks and precipitating tau spread (Vasconcelos et al., 2016). The role of microglial activation is likely to be critical in this process – for example, microglial cells activated by amyloid plaques may induce further tau hyperphosphorylation, inducing further neurofibrillary tangles and initiating tau spread across the cortex, leading to Alzheimer's disease (represented in figure 6). It is important to note that not all areas follow this model, and imaging data may not fully reflect the spectrum of heterogeneity of pathology in Alzheimer's disease. Hopefully, autoradiographic and histopathological follow up of our imaging dataset will provide support for this hypothesis.

Microglial activation may at times play a protective role: a mouse study crossing transgenic amyloid and transgenic tau mice produced offspring with increased microglial activation (and increased phagocytic ability), and a 40-50% reduced plaque load, implying that under certain circumstances tau –induced microglia activation clears amyloid load (Chen et al., 2016). However, current PET tracers are unable to differentiate between protective or detrimental roles of activated microglia.

The use of ^{11}C-PBR28 PET as a marker of TSPO expression and, indirectly, microglial activation should also be discussed. ^{11}C-PBR28 has a subnanomolar affinity for a binding site on TSPO expressed by the mitochondria of activated microglia which is eighty times higher than the affinity of the first generation ligand ^{11}C-PK11195 (Kreisl et al., 2010). It has differentiated Alzheimer's disease from healthy controls in several studies (Kreisl et al., 2013; Lyoo, 2015) but no studies to date have shown increased uptake in mild cognitive impairment subjects. Binding has been shown to increase with Alzheimer disease progression (Kreisl et al., 2016), and has been shown to correlate with extent of neurodegeneration in the primary visual cortex of Posterior Cortical Atrophy cases. (Kreisl 2017). However, there are also limitations. No studies to date have shown group regional V_T differences between AD, MCI and controls. *High variability is also a feature of ^{11}C-PBR28 PET(Cumming et al., 2018)): A study in healthy controls showed high test-retest variability (15.9+/-12.2%), high inter-subject variability and significant differences in results when scanning the same subjects in the morning and afternoon (Collste et al., 2016). However, another study examining 11C-PBR28 in multiple sclerosis found a lower absolute mean test-retest variability ranging from 7-9%. (Park et al., 2015)*. Other studies have shown that there are significant correlations between peripheral leucocyte count and brain TSPO binding, suggesting that TSPO expression may be susceptible to systemic immune changes. (Kanegawa et al., 2016) The variable free fraction of tracer in the plasma may introduce

another source of variance. This variability may be one reason for the lack of group differences between the AD group and healthy controls in our cohort. Moreover, a blocking study showed tracer binding throughout the brain, indicates that there is no region in the brain that is truly devoid of binding that can be used as a reference for non-specific binding (Owen et al., 2014).

Furthermore, there is evidence that levels of microglial activation fluctuate with Alzheimer's disease progression(Fan et al., 2017). There is evidence of increased microglial activation early on(Hamelin et al., 2016), which plateaus(Lopez-Picon et al., 2017), followed by further activation later in the disease course(Fan et al., 2017). Our cohort was imaged at a single time point so it is not possible to ascertain the exact stage of disease trajectory that each individual is on, with a mean MMSE score of 22, our AD cohort had relatively mild or 'intermediate' disease, which may also explain the low levels of microglial activation in some individuals and the lack of group difference.

The TSPO receptor is used as a biomarker marker for neuroinflammation but, as well as being expressed by activated microglia, TSPO can also become upregulated in other cells including astroglia and neurons. It is possible that the correlations we see with PBR28 PET between intra-cellular tau tangle and activated microglia load reflect TSPO expression by dystrophic neurons, however, histopathological studies on Alzheimer brains would be against this. Rather, our results are in line with histopathological studies that show activated microglia surround neurofibrillary tangles (Sheffield, 2000; Serrano-Pozo et al., 2011b). Autoradiographic studies are required to confirm that our results do not represent false-positive co-localisation. Finally, a recent study examining the effects of myeloid cell activation on TSPO expression found that activation of pro-inflammatory macrophages in humans is associated with a reduction in TSPO expression (in contrast to rodents, where the converse was seen) (Owen et al., 2017). This study indicates a possible limitation in using the TSPO receptor as a neuroinflammation marker.

Several different analytical methods have been used with ^{11}C-PBR28 PET. Studies have reported conflicting results, which is partly due to different methodological approaches. Groups have corrected V_T for the free fraction of ^{11}C-PBR28 in plasma and reported significant differences between patients and control subjects (Kreisl et al., 2013). Other groups have used the cerebellum as a 'pseudo-reference region', arguing that Alzheimer pathology occurs late in the cerebellum so any pathological changes in early cases will be

seen in the isocortex. (Lyoo, 2015). Groups using ^{11}C-PBR28 PET to study other diseases have used 'whole brain binding' as a reference region (Bloomfield et al., 2016) in order to reduce variance due to genotypic and plasma protein binding variability. However, as there is no cortical region devoid of translocator protein, this approach will act to diminish observed relative changes in target regions. A whole brain reference region of interest will also reflect signal from white matter and subcortical structures (Narendran and Frankle, 2016).

Another factor to consider with ^{11C}-PBR28 is correction for free fraction of the tracer in plasma (fP, which may account for some of the variability introduced by plasma input function).

In our cohort, fP ranged from 0.78% to 2.89%, and there were no significant differences in fP between the three groups. (mean value for free fraction of tracer in plasma = 1.829, standard deviation 0.478; coefficient of variation 26%). This high variability is similar to previous reports (Hines et al., 2013; Rizzo et al., 2014). Some authors argue that the very small values of fP can lead to inaccuracies in measurement and laboratory error. (Rizzo et al., 2014; Turkheimer et al., 2015). The effect of fP levels only becomes critical, however, if exchange rates of ^{11}C-PBR28 on and off plasma proteins is of the same order or slower than its rate of brain uptake. Generally exchange of tracers on and off plasma proteins is rapid compared to rates of their brain uptake and so has relatively little influence on brain VTs. Having said that, a study using ^{11}C-PK11195 found that this isoquinoline tracer strongly bound to some plasma proteins which are upregulated in inflammatory diseases. (Lockhart et al., 2003) This may confound measurement of TSPO binding in inflammatory diseases such as Alzheimer's disease.

As such, and in view of the lack of consensus agreement about whether V_T or V_T/fP is superior, (Cumming et al., 2018) we have reported V_T (rather than V_T/fP).

Thus, it is clear that there are limitations associated with the use of ^{11}C-PBR28 PET, and results should be interpreted with caution. In view of the fact that there is no true reference region in the brain for TSPO binding, we chose to compute absolute quantification using an arterial plasma input function as this remains the gold standard for PET analysis.

One of the strengths of our study is that our disease groups were clinically well characterised with detailed neuropsychometric evaluation and known amyloid status. In addition, we used an arterial input function to analyse ^{11}C-PBR28 V_T. We also accounted for the differential

binding status of subjects for ^{11}C-PBR28 due to differential expression of TSPO polymorphisms (Owen et al., 2012; Kreisl, 2013; Yoder et al., 2013) by creating z-maps for each individual's binding compared to the controls. This allowed all subjects to be examined as a group whether classified as MAB or HAB. We excluded the low affinity binders from the study (due to their negligible binding) but it has recently been demonstrated that binding status is not associated with clinical status, therefore conclusions from a subgroup can be applied to a whole cohort. (Fan, 2015) However, the spectrum in binding affinity remains a limitation of the second generation TSPO tracers, and other unidentified genetic sources of variation may also be present.

One of the limitations of our study was that for the ^{11}C-PBR28 and ^{18}F-flutemetamol PET scans, the mild cognitive impairment and Alzheimer's disease groups were significantly older than our healthy control group. While some studies have suggested that microglial activation increase with age (Kumar et al., 2012; Walker et al., 2015), other PET studies have not detected a significant increase with age (Suridjan et al., 2014). Additionally, we did not find a correlation between microglial activation and age in our healthy control group. Secondly, due to patient and scanner availability and the onerous nature of the study, there were time delays between scans. During these months, the pathological processes may have progressed, but we assume this would not have been considerable given the long duration of these processes.

Individuals taking benzodiazepines were excluded from the study. One individual in the Alzheimer's disease group was taking a non steroidal anti-inflammatory medication and it was not recorded whether a dose was taken on the day of the scan. This may represent a potential confound affecting ^{11}C-PBR binding, although this individual had significantly higher uptake than the mean +2 standard deviations of the control group.

Additionally, while the correlations between tracer binding in this cohort are intriguing, we acknowledge the fact that there were no significant between group mean differences between the Alzheimer's disease group and amyloid negative group and healthy controls. This is a limitation of the study, and may be due to the high variability in ^{11}C-PBR28 described above, the dynamic nature of microglial activation or the fact that the study is small and underpowered to detect group level differences, particularly when subdividing groups according to amyloid status, disease group and binding status. However, our sub-group analysis of tracer positive individuals confirmed that correlations across tracer uptake did not artefactually arise from 'null data points' from tracer negative individuals.

We acknowledge that the numbers used in the study are too small to make a definitive conclusion about the distribution of these processes in Alzheimer's disease. This is particularly apparent when dividing groups according to disease status and amyloid status. If we had larger numbers of individuals with increased binding of all three tracers, a more robust correlative analysis could be performed. However these findings are important and may guide future work in this direction.

It should also be noted that while we have demonstrated correlations between tracer binding, off-target binding has been reported for ^{18}F-AV1451 in the midbrain, lateral geniculate nucleus, choroid plexus, basal ganglia, substantia nigra, meninges, retina and melanin containing cells (Marquie et al., 2015; Lowe et al., 2016). However, this off-target binding is also likely to be present in both patients and controls and the interrogation of Z-score maps should help correct for this.

Finally, recent work has shown that ^{18}F-flutemetamol only detects later stages of amyloid deposition, universally missing Thal stages 1 and 2, and some Thal stage 3 cases (Thal et al., 2015). Consequently, some of the individuals in our 'amyloid negative' group could have had early Alzheimer's pathology, biasing correlations between tau and microglial activation towards a positive outcome.

Implications and future directions

Our findings suggest that levels of microglial activation can correlate with tau tangle and amyloid plaque load in mild cognitive impairment and Alzheimer's disease. This suggests that microglial activation may play a role in propagating disease pathology in Alzheimer's disease. Certain areas of the brain are clearly more vulnerable to Alzheimer's pathology - microglial activation correlated with both amyloid deposition and tau aggregation in the posterior temporal lobe and superior frontal gyrus.

An important further area of study would focus on the cognitively healthy older control group, to detect tracer binding and pathological correlations not yet reaching clinical significance.

Further longitudinal studies in these subjects to evaluate the progression and distribution of the pathologies would allow us to better understand their underlying temporal inter-relationships.

Conclusion

This is the first PET study to examine pathological correlations between levels of microglial activation and aberrant protein aggregation in mild cognitive impairment and Alzheimer's disease. We found that microglial activation correlates strongly with tau aggregation in established Alzheimer disease and, to a lesser extent with amyloid deposition. In contrast, microglial activation correlates more strongly with amyloid deposition in MCI. These findings support previous in vitro findings and confirm the complex relationships between these pathological processes in Alzheimer's disease. Our findings suggest that a multi-targeted approach will be necessary for an effective therapeutic intervention.

Figures and tables

Table 1 Demographics of the study cohort

Figure 1 Voxel level increases in ^{18}F-flutemetamol (Fig 1A and 1B), ^{18}F-AV1451 (Fig1C, 1D and 1E) and ^{11}C-PBR28 High Affinity Binders (Fig1F, 1G and 1H) compared to the healthy controls using independent t-test in SPM. For ^{18}F-flutemetamol and ^{11}C-PBR28, a threshold of significance of $p<0.05$ was used. For ^{18}F-AV1451, a threshold of significance of $p<0.01$ was used. These images show the distribution of pathology in the mild cognitive impairment and Alzheimer's disease groups.

Figure 2 Voxel level correlations between tau and microglial activation in the amyloid positive mild cognitive impairment (Fig 2A), Alzheimer's disease (Fig 2B) and amyloid negative cognitively impaired individuals (Fig 2C)

Figure 3 Voxel level correlations between amyloid and microglial activation in the amyloid positive mild cognitive impairment (Fig 3A) and Alzheimer's disease (Fig 3B) individuals

Figure 4 Voxel level correlations in the tracer positive individuals only, between microglial activation and tau aggregation (Figure 4A) and microglial activation and amyloid deposition (Figure 4B).

Figure 5 Individual parametric maps (Individual 1-9) of microglial activation (A) and tau aggregation (B) in the nine amyloid negative individuals with cognitive impairment, compared to the control mean. Clusters show trends of increased binding. Individuals 1,2,4,5 and 6 had statistically significant clusters of ^{18}F-AV1451 binding, while individuals 1,2,3,4 and 6 had statistically significant ^{11}C-PBR28 binding compared to the control groups. This

figure is provided to illustrate distributions of the pathologies in this small group of individuals.

Figure 6 The vicious cycle of activated microglia and protein aggregation. Activated microglia surround amyloid plaque and neurofibrillary tangles, and in turn promote upregulation of amyloid plaque and tangles. Further, the pro-inflammatory products of activated microglia promote further tau hyperphosphorylation and spreading of neurofibrillary tangles throughout the cortex

Acknowledgements

The authors thank Imanova Centre for Imaging Sciences for the provision of ^{11}C-PBR28, scanning and blood analysis equipment, and the Imperial College Clinical Imaging Facility for PET and MRI scan facilities. We thank GE Healthcare for the provision of ^{18}F-flutemetamol and Avid pharmaceuticals for use of the radiotracer ^{18}F-AV1451. The PET scans and MRI scans were funded by the Medical Research Council and Alzheimer's Research UK. This article presents independent research funded by Medical Research Council and Alzheimer's Research, UK. The study was supported by the National Institute for Health Research Clinical Research Facility at Imperial College Healthcare NHS Trust.

Funding

The PET scans and MRI scans were funded by the Medical Research Council (grant number WMCN_P33428) and part of the study was funded by Alzheimer's Research UK (grant number WMCN_P23750).

Conflicts of interest

Dr. Edison was funded by the Medical Research Council and now by Higher Education Funding Council for England (HEFCE). He has also received grants from Alzheimer's Research, UK, Alzheimer's Drug Discovery Foundation, Alzheimer's Society, UK, Novo Nordisk, Piramal Life Sciences and GE Healthcare. He is also a consultant to Pfizer. Prof. Brooks has received research grants and non-financial support from the Medical Research Council, grants from Alzheimer's Research Trust, during the conduct of the study; other from GE Healthcare, personal fees from AstraZeneca, Cytox, Shire, Novartis, GSK, Navidea, UCB, and Acadia, along with grants from Michael J Fox Foundation, European Commission,

the Danish council for Independent Research, and the Lundbeck Foundation outside the submitted work.

Supplementary information

Supplementary Table 1 Clusters of positive correlations between ^{11}C-PBR 28 and ^{18}F-AV1451 and ^{18}F-flutemetamol

Supplementary Table 2a Clusters of voxel-level positive correlation between ^{18}F-Flutemetamol and ^{11}C-PBR28 in individuals positive for all 3 tracers

Supplementary Table 2b Voxel level comparisons between the tracer positive individuals and healthy controls for each tracer

Supplementary Table 3 Clusters of positive correlation between ^{11}C-PBR28 and ^{18}F-AV1451 and ^{18}F-flutemetamol after partial volume correction

Supplementary table 4 Individual clusters of increased binding of ^{18}F-AV1451 and ^{11}C-PBR28. In the Alzheimer's disease group (all of whom were amyloid positive), five had increased tau and microglial activation; nine had increased tau. In the amyloid positive mild cognitive impairment group, four had increased tau, while two had increased microglial activation and one had increased tau and microglial activation. In the amyloid negative group, three individuals had increased tau and microglial activation, two had increased microglial activation and one had increase tau only.

Supplementary Figure 1 Mean colourmap images for controls, mild cognitive impairment and Alzheimer's disease individuals for all three processes. Figures 4A-4D show mean ^{18}F-AV1451 uptake (controls, mild cognitive impairment, Alzheimer's disease, Amyloid negative individuals respectively); Figures 4E-4H show ^{11}C-PBR28 (controls, mild cognitive impairments, Alzheimer's disease, Amyloid negative individuals, respectively) and Figures 4I to 4K show mean ^{18}F-flutemetamol uptake (controls, mild cognitive impairment and Alzheimer's disease).

Supplementary Figure 2 Partial volume corrected positive correlations between ^{11}C-PBR28 and ^{11}F-flutemetamol in mild cognitive impairment (A) and Alzheimer's disease (B), and between ^{11}C-PBR28 and ^{18}F-AV1451 in mild cognitive impairment (C), Alzheimer's disease (D) and the amyloid negative cognitively impaired individuals (E)

Supplementary Figure 3a Correlation plots of individual voxel binding between ^{11}C-PBR28 and ^{18}F-AV1451 in the mild cognitive impairment group (Figures A and B))

Supplementary Figure 3b Correlation plots of individual voxel binding between ^{11}C-PBR28 and ^{18}F-AV1451 in the Alzheimer's disease (Figures C, D and E) and amyloid negative individuals (Figure F).

Supplementary Figure 3c Correlations between ^{18}F-flutemetamol and ^{11}C-PBR28 are shown in the mild cognitive impairment group (Figures G and H) and Alzheimer's disease (Figure I).

Supplementary Figure 4 Healthy control logan VD values in the high affinity binders (Fig 4A) and in comparison with mild cognitive impairment and Alzheimer's disease in the composite cortex (Fig 4B). Figs 4C and 4D shows control data in the medium affinity binders, and comparison with the mild cognitive impairment and Alzheimer's disease in the composite cortex.

References

Craig-Schapiro, R, Perrin RJ, Roe CM, Xiong C, Carter D, Cairns NJ; A Novel Prognostic Fluid Biomarker for Preclinical Alzheimer's Disease. Biol Psychiatry 2010; 68(10):903-12

Bloomfield PS, Selvaraj S, Veronese M, Rizzo G, Bertoldo A, Owen DR*, et al.* Microglial activity in people at ultra high risk of psychosis and in schizophrenia; an [11C]PBR28 PET brain imaging study. Am J Psychiatry 2016; 173(1): 44-52.

Braak H, Braak E. Neuropathological Staging of Alzheimer Related Changes in Alzheimer's Disease. Acta Neuropathol 1991; 82: 239-59.

Cagnin A, Rossor M, Sampson EL, MacKinnon T, Banati R. In vivo detection of microglial activation in frontotemporal dementia. Ann Neurol 2004; 56(6): 894-7.

Casanova R, Ryali S, Baer A, Laurienti PJ, Burdette JH, Hayasaka S*, et al.* Biological Parametric Mapping: A Statistical Toolbox for Multi-Modality Brain Image Analysis. NeuroImage 2007; 34(1): 137-43.

Chen W, Abud EA, Yeung ST, Lakatos A, Nassi T, Wang J*, et al.* Increased tauopathy drives microglia-mediated clearance of beta-amyloid. Acta Neuropathol Commun 2016; 4(1): 63.

Collste K, Forsberg A, Varrone A, Amini N, Aeinehband S, Yakushev I*, et al.* Test-rest reproducibility of [(11)C]PBR28 binding to TSPO in healthy control subjects. Eur J Nucl Med Mol Imaging 2016; 43(1): 173-83.

Crary JF, Trojanowski JQ, Schneider JA, Abisambra JF, Abner EL, Alafuzoff I*, et al.* Primary age-related tauopathy (PART): a common pathology is associated with human aging. Acta Neuropathol 2014; 128(755-766).

Cumming P, Burgher B, Patkar O, Breakspear M, Vasdev N, Thomas P*, et al.* Sifting through the surfeit of neuroinflammation tracers. J Cereb Blood Flow Metab 2018; 38(2): 204-24.

Fan Z, Brooks DJ, Okello A, Edison P. An early and late peak in microglial activation in Alzheimer's disease trajectory. Brain 2017; 140(3): 792-803.

Fan Z, Calsolaro V, Atkinson RA, Femminella GD, Waldman A, Buckley C*, et al.* Flutriciclamide (18F-GE180) PET: first in-human PET study of novel third generatino in vivo marker of human translocator protein. J Nucl Med 2016; 57(11): 1753-9.

Fan ZH, D; Pasqualetti, G; Williams, J; Brooks, DJ; Edison, P. Can studies of neuroinflammation in a TSPO genetic subgroup (HAB or MAB) be applied to the entire AD cohort? J Nucl Med 2015; 56(5):707-13

Gorlovoy P, Larionov S, Pham TT, Neumann H. Accumulation of tau induced in neurites by microglial proinflammatory mediators. FASEB J 2009; 23(8): 2502-13.

Hamelin L, Lagrade J, Dorothee G, Leroy C, Labit M, Comley RA*, et al.* Early and Protective microglial activation in Alzheimer's disease: a prospective study using 18F-DPA-714 PET imaging. Brain 2016; 139: 1252-64.

Hammers AA, R; Koepp, M; Free, S; Myers, R; Lemieux, L; Mitchell, T; Brooks, DJ; Duncan, JS. Three-dimensional maximum probability atlas of the human brain, with particular reference to the temporal lobe. Hum Brain Mapp 2003; 19(4): 224-47.

Heneka MT, Carson MJ, Khoury JE, Landreth GE, Brosseron F, Feinstein DL*, et al.* Neuroinflammation in Alzheimer's disease. Lancet Neurol 2015; 14(4): 388-405.

Hines CS, Fujita M, Zoghbi SS, Kim JS, Quezado Z, Herscovitch P*, et al.* Propofol decreases in vivo binding of 11C-PBR28 to translocator protein (18 kDa) in the human brain. J Nucl Med 2013; 54(1): 64-9.

Ikonomovic MD, Buckley CJ, Heurling K, Sherwin P, Jones PA, Zanette M*, et al.* Post-mortem histopathology underlying beta-amyloid PET imaging following flutemetamol F 18 injection. Acta Neuropathol Commun 2016; 4(1): 130.

Ishizawa K, Dickson D. Microglial Activation Parallels System Degeneration in Progressive Supranuclear Palsy and Corticobasal Degeneration. J Neuropath Exp Neurol 2001; 60(6): 647-57.

Ishizawa K, Komori T, Sasaki S, Arai N, Mizutani T, Hirose T. Microglial activation parallels system degeneration in multiple system atrophy. J Neuropath Exp Neurol 2004; 63(1): 43-52.

Kanegawa N, Collste K, Forsberg A, Schain M, Arakawa R, Jucaite A*, et al.* In vivo evidence of a functional association between immune cells in blood and brain in healthy human subjects. Brain Behav Immun 2016; 54: 149-57.

Kreisl WC, Fujita M, Fujimura Y, Kimura N, Jenko KJ, Kannan P*, et al.* Comparison of [(11)C]-(R)-PK 11195 and [(11)C]PBR28, two radioligands for translocator protein (18 kDa) in human and monkey: Implications for positron emission tomographic imaging of this inflammation biomarker. NeuroImage 2010; 49(4): 2924-32.

Kreisl WC, Lyoo CH, Liow JS, Wei M, Snow J, Page E*, et al.* (11)C-PBR28 binding to translocator protein increases with progression of Alzheimer's disease. Neurobiol Ageing 2016(44): 53-61.

Kreisl WC, Lyoo CH, McGwier M, Snow J, Jenko KJ, Kimura N*, et al.* In vivo radioligand binding to translocator protein correlates with severity of Alzheimer's disease. Brain 2013; 136(Pt 7): 2228-38.

Kreisl WCJ, K; Hines, C; Lyoo, C; Corona, W; Morse, C; Zoghbi, S; Hyde, T; Kleinman, J; Pike, J; McMahon, F; Innis, and the Biomarkers Consortium PET Radioligand Project Team. A genetic polymorphism for translocator protein 18kDa affects both in vitro and in vivo radioligand binding in human brain to this putative biomarker of neuroinflammation. J Cereb Blood Flow Metab 2013; 33(1): 53-8.

Kumar A, Muzik O, V S, Chugani D, Chakraborty P, Chugani HT. Evaluation of age-related changes in translocator protein (TSPO) in human brainusing (11)C-[R]-PK11195 PET. J Neuroinflammation 2012; 9(232).

Lee DC, Rizer J, Selenica ML, Reid P, Kraft C, Johnson A*, et al.* LPS- induced inflammation exacerbates phospho-tau pathology in rTg4510 mice. J Neuroinflammation 2010; 7: 56.

Lee M, McGeer E, McGeer PL. Activated human microglia stimulate neuroblastoma cells to upregulate production of beta amyloid protein and tau: implications for Alzheimer's disease pathogenesis. Neurobiol Aging 2015; 36(1): 42-52.

Lockhart A, Davis B, Matthews JC, Rahmoune H, Hong G, Gee A*, et al.* The peripheral benzodiazepine receptor ligand PK11195 binds with high affinity to the acute phase reactant α1-acid glycoprotein: implications for the use of the ligand as a CNS inflammatory marker. Nucl Med Biol 2003; 30(2): 199-206.

Logan J. Graphical analysis of PET data applied to reversible and irreversible tracers. Nucl Med Biol 2000; 27(7): 661-70.

Lopez-Picon FR, Snellman A, Eskola O, Helin S, Solin O, Haaparanta-Solin M*, et al.* Neuroinflammation appears early and then pleatueas in a mouse model of Alzheimer's disase shown by PET imaging. J Nucl Med 2018; 59(3):509-15.

Lowe VJ, Curran G, Fang P, Liesinger AM, Josephs KA, Parisi JE*, et al.* An autoradiographic evaluation of AV-1451 Tau PET in dementia. Acta Neuropathol Commun 2016; 4(1): 58.

Lyoo CI, M; Liow, JS; Zoghbi, SS; Morse, C; Pike VW; Fujita, M; Innis, RB; Kreisl, WC. Cerebellum can serve as a pseudo-reference region in Alzheimer's Disease to detect

neuroinflammation measured with PET radioligand binding to translocator protein (TSPO). Journal of Nuclear Medicine 2015;56 (5):701-6

Manso Y, Holland PR, Kitamura A, Szymkowiak S, Duncombe J, Hennessy E*, et al.* Minocycline reduces microgliosis and improves subcortical white matter function in a model of cerebral vascular disease. Glia 2018; 66(1):34-46.

Maphis N, Guixiang X, Kokiko-Cochran ON, Cardona AE, Ransohoff RM, Lamb BT*, et al.* Loss of tau rescues inflammation-mediated neurodegeneration. Front Neurosci 2015a; 9(196).

Maphis N, Xu G, Kokiko-Cochran ON, Jiang S, Cardona A, Ransohoff RM*, et al.* Reactive microglia drive tau pathology and contribute to the spreading of pathological tau in the brain. Brain 2015b; 138(Pt 6): 1738-55.

Marquie M, Normandin MD, Vanderburg CR, Costantino IM, Bien EA, Rycyna LG*, et al.* Validating novel tau positron emission tomography tracer [F-18]-AV-1451 (T807) on postmortem brain tissue. Ann Neurol 2015; 78(5): 787-800.

McGinnity CJ, Riano Barros DA, Rosso L, Veronese M, Rizzo G, Bertoldo A*, et al.* Test-retest reproducibility of quantitative binding measures of [(11)C]Ro15-4513, a PET ligand for GABAA receptors containing alpha5 subunits. Neuroimage 2017; 152: 270-82.

McKhann GM, Drachman D, Folstein M, Katzman R, Price D, E.M. S. Clinical diagnosis of Alzheimer's disease: report of the NINCDS-ADRDA Work Group under the auspices of the Department of Healthy and Human Services Task Force on Alzheimer's Disease. Neurology 1984; 34(7): 939-44.

McKhann GM, Knopman DS, Chertkow H, Hyman BT, Jack CR, Jr., Kawas CH*, et al.* The diagnosis of dementia due to Alzheimer's disease: recommendations from the National Institute on Aging-Alzheimer's Association workgroups on diagnostic guidelines for Alzheimer's disease. Alzheimers Dement 2011; 7(3): 263-9.

Narendran R, Frankle WG. Comment on Analyses and Conclusions of 'Microglial Activity in People at Ultra High Risk of Psychosis and in Schizophrenia: an [11C]PBR28 PET Brain Imaging Study. Am J Psychiatry 2016; 173: 535-6.

Owen DR, Guo Q, Kalk NJ, Colasanti A, Kalogiannopoulou D, Dimber R*, et al.* Determination of [(11)C]PBR28 binding potential in vivo: a first human TSPO blocking study. J Cereb Blood Flow Metab 2014; 34(6): 989-94.

Owen DR, Narayan N, Wells L, Healy L, Smyth E, Rabiner EA*, et al.* Pro-inflammatory activation of primary microglia and macrophages increases 18kDa translocator expression in rodents but not humans. J Cereb Blood Flow Metab 2017; 37(8): 2679-90.

Owen DR, Yeo AJ, Gunn RN, Song K, Wadsworth G, Lewis A, *et al.* An 18-kDa translocator protein (TSPO) polymorphism explains differences in binding affinity of the PET radioligand PBR28. J Cereb Blood Flow Metab 2012; 32(1): 1-5.

Park E, Gallezot JD, Delgadillo A, Liu S, Planeta B, Lin SF, *et al.* C-PBR28 imaging in multiple sclerosis patients and healthy controls: test-retest reproducibility and focal visualization of active white matter areas. Eur J Nucl Med Mol Imaging 2015; 42:1081-92.

Pascoal TA, Mathotaarachchi S, Shin M, Benedet AL, Mohades S, Wang S, *et al.* Synergistic interaction between amyloid and tau predicts the progression to dementia. Alzheimers Dement 2017; 13(6):644-653

Pasqualetti G, Brooks DJ, Edison P. The role of neuroinflammation in dementias. Curr Neurol Neurosci Rep 2015; 15(4): 17.

Paulus W, Bancher C, Jellinger K. Microglial reaction in Pick's disease. Neurosci Lett 1993; 161: 89-92.

Perl DP. Neuropathology of Alzheimer's Disease. Mt Sinai J Med 2010; 77(1).

Perlmutter LB, E; Chui, H. Morphologic association betweem microglia and senile plaque amyloid in Alzheimer's Disease. Neurosci Lett 1990; 119: 32-6.

Petersen RC, Caracciolo B, Brayne C, Gauthier S, Jelic V, Fratiglioni L. Mild cognitive impairment: a concept in evolution. J Intern Med 2004; 275(3): 214-28.

Pontecorvo MJ, Devous MD, Sr., Navitsky M, Lu M, Salloway S, Schaerf FW, *et al.* Relationships between flortaucipir PET tau binding and amyloid burden, clinical diagnosis, age and cognition. Brain 2017; 140(3):748-763.

Price J, Morris J. Tangles and Plaques in Nondemented Aging and 'Preclinical' Alzheimer's Disease. Ann Neurol 1999; 45(3): 358-68.

Quintanilla RA, Orellana D, Gonzalez-Billault C, Maccioni R. Interluekin-6 induces Alzheimer-type phosphorylation of tau protein by deregulating the cdk5/p35 pathway. Exp Cell Res 2004; 295: 245-57.

Rizzo G, Veronese M, M T, Zanotti-Fregonara P, Turkheimer FE, A B. Kinetic modeling without accounting for the vascular component impaires the quantificatio of 11C-PBR28 brain PET data. J Cereb Blood Flow Metab 2014(34): 1060-9.

Salloway S, Sperling R, Fox NC, Blennow K, Klunk W, Raskind M, *et al.* Two phase 3 trials of bapineuzumab in mild-to-moderate Alzheimer's disease. New Engl J Med 2014; 370(4): 322-33.

Schneider JA, Arvanitakis Z, Leurgans SE, Bennett DA. The Neuropathology of Probable Alzheimer's Disease and Mild Cognitive Impairment. Ann Neurol 2009; 66(2): 200-8.

Serrano-Pozo A, Betensky RA, Frosch MP, Hyman BT. Plaque-Associated Local Toxicity Increases over the Clinical Course of Alzheimer Disease. American J Pathol 2016; 186(2): 375-84.

Serrano-Pozo A, Frosch MP, Masliah E, Hyman BT. Neuropathological alterations in Alzheimer disease. Cold Spring Harb Perspect Med 2011a; 1(1): a006189.

Serrano-Pozo A, Mielke ML, Gomez-Isla T, Betensky RA, Growdon JH, Frosch MP*, et al.* Reactive glia not only associates with plaques but also parallels tangles in Alzheimer's disease. Am J Pathol 2011b; 179(3): 1373-84.

Serrano-Pozo A, Qian J, Monsell SE, Blacker D, Gomez-Isla T, Betensky RA*, et al.* Mild to Moderate Alzheimer Dementia with Insufficient Neuropathological Changes. Ann Neurol 2014; 75: 597-601.

Sheffield LM, J; Berman, N. Regional distribution of cortical microglia parallels that of neurofibrillary tangles in Alzheimer's disease. Neurosci Lett 2000; 285: 165-8.

Shidahara M, Tsoumpas C, Hammers A, Boussion N, Visvikis D, Suhara T*, et al.* Functional and structural synergy for resolution recovery and partial volume correction in brain PET. NeuroImage 2009; 44(2): 340-8.

Stalder M, Phinney A, Probst A, Sommer B, Staufenbiel M, Jucker M. Association of Microglia with Amyloid Plaques in Brain of APP23 Transgenic Mice. Am J Pathol 1999; 154(6): 1673-84

Surendranathan A, Rowe JB, O'Brien JT. Neuroinflammation in Lewy body dementia. Parkinsonism Relat Disord 2015; 21(12): 1398-406.

Suridjan I, P.M. R, Voineskos AN, Selvanathan T, Setiawan E, Strafella AP*, et al.* Neuroinflammation in healthy aging: a PET study using a novel Translocator Protein 18kDa (TSPO) radioligand [(18)F]-FEPPA. NeuroImage 2014; 1(84): 868-75.

Thal DR, Beach TG, Zanette M, Heurling K, Chakrabarty A, Ismail A*, et al.* [(18)F]flutemetamol amyloid positron emission tomography in preclinical and symptomatic Alzheimer's disease: specific detection of advanced phases of amyloid-B pathology. Alzheimers Dement 2015; 11(8): 975-85.

Turkheimer FE, Rizzo G, Bloomfield PS, Howes O, Zanotti-Fregonara P, Bertoldo A*, et al.* The methodology of TSPO imaging with positron emission tomography. Biochem Soc Trans 2015; 43(4): 586-92.

Vasconcelos B, Stancu IC, Buist A, Bird M, Wang P, Vanoosthuyse A*, et al.* Heterotypic seeding of Tau fibrillization by pre-aggregated Abeta provides potent seeds for prion-like seeding and propagation of Tau-pathology in vivo. Acta Neuropathol 2016; 131(4): 549-69.

Vidale S, Consoli A, Arnaboldi M, Consoli D. Postischemic Inflammation in Acute Stroke. J Clin Neurol 2017; 13(1): 1-9.

Villemagne V, Burnham S, Bourgeat P, Brown B, Ellis K, Salvado O*, et al.* Amyloid B deposition, neurodegeneration, and cognitive decline in sporadic Alzheimer's Disease: a prospective cohort study. Lancet 2013; 12: 357-67.

Walker MD, Dinelle K, Kornelsen R, Lee NV, Miao Q, Adam M*, et al.* [C]PBR28 PET imaging is sensitive to neuroinflammation in the aged rat. J Cereb Blood Flow Metab 2015; 35(8):1331-8

Xia CF, Arteaga J, Chen G, Gangadharmath U, Gomez LF, Kasi D*, et al.* [(18)F]T807, a novel tau positron emission tomography imaging agent for Alzheimer's disease. Alzheimers Dement 2013; 9(6): 666-76.

Yoder KK, Nho K, Risacher SL, Kim S, Shen L, Saykin AJ. Influence of TSPO genotype on 11C-PBR28 standardized uptake values. J Nucl Med 2013; 54(8): 1320-2.

Yoshiyama Y, Higuchi M, Zhang B, Huang SM, Iwata N, Saido TC*, et al.* Synapse loss and microglial activation precede tangles in a P301S tauopathy mouse model. Neuron 2007; 53(3): 337-51.

Zhao SC, Ma LS, Chu ZH, Xu H, Wu WQ, Liu F. Regulation of microglial activation in stroke. Acta Pharmacol Sin 2017; 38(4): 445-58.

Zilka N, Stozicka Z, Kovac A, Pilipcinec E, Bugos O, Novak M. Human misfolded truncated tau protein promotes activation of microglia and leukocyte infiltration in the transgenic rat model of tauopathy. J Neuroimmunol 2009; 209(1-2): 16-25.

Table 1 Demographics of the study cohort

	Controls (n=19)	Amyloid positive mild cognitive impairment (n=9)	Amyloid negative mild cognitive impairment (n=7)	Alzheimer's disease (n=16)
Age	64.22(8.52)	76.62(5.07)**	68.71(7.48)	73.69(7.15)*
Years education	13.37(3.34)	14.14(3.98)	11.25(0.96)	12.92(2.74)
Mini Mental State Examination (total = 30)	29.41(1.06)	28.33(1.22)	26.71(2.06)*	21.62(3.28)**
Delayed visual recall (total = 36)	18.18(7.12)	10.44(6.32)*	19.29(3.67)	5.19(6.33)**
Delayed word list recall (total = 12)	10.21(2.04)	2.22(1.99)**	6.86(3.34)*	1.14(1.70)**
Word list recognition (total = 12)	11.27(1.03)	7.67(3.57)	8.29(3.63)	3.64(3.13)
Semantic fluency	20.73(6.00)	13.33(4.03)*	19.29(5.82)	10.93(6.13)**
Trail-making A	35.24(10.83)	51.22(11.71)	52.43(25.44)*	107.67(120>
Trail-making B	74.13(23.0)	171.67(106)**	116.33(39.80)**	148(46)*
Right hippocampal volume (mm^3)	3860(407)	3398(574)	3669(477)	2827(549)**

Left hippocampal volume (mm^3)	3745(333)	3199(779)*	3662(267)	2743(400)**
White matter hypointensity volume (mm^3)	2160(1208)	3693.5(1771)	9898(18658)	5153(3296)**

** p<0.01, * p<0.05

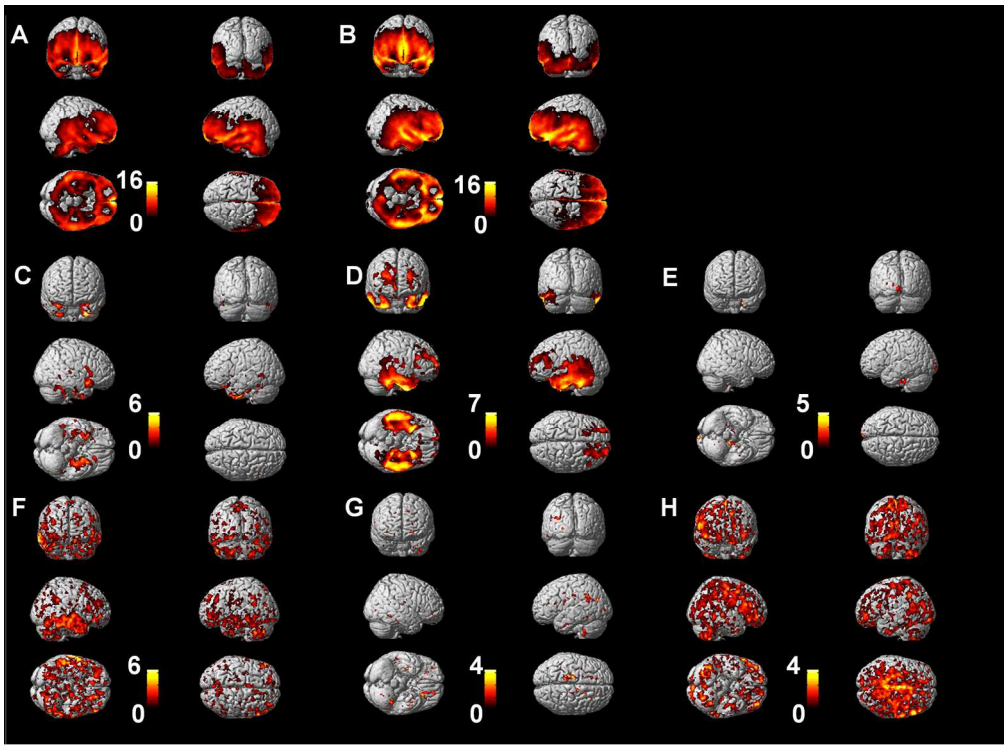

Figure 1 Voxel level increases in 18F-flutemetamol (Fig 1A and 1B), 18F-AV1451 (Fig1C, 1D and 1E) and 11C-PBR28 High Affinity Binders (Fig1F, 1G and 1H) compared to the healthy controls using independent t-test in SPM. For 18F-flutemetamol and 11C-PBR28, a threshold of significance of $p<0.05$ was used. For 18F-AV1451, a threshold of significance of $p<0.01$ was used. These images show the distribution of pathology in the mild cognitive impairment and Alzheimer's disease groups

184x136mm (300 x 300 DPI)

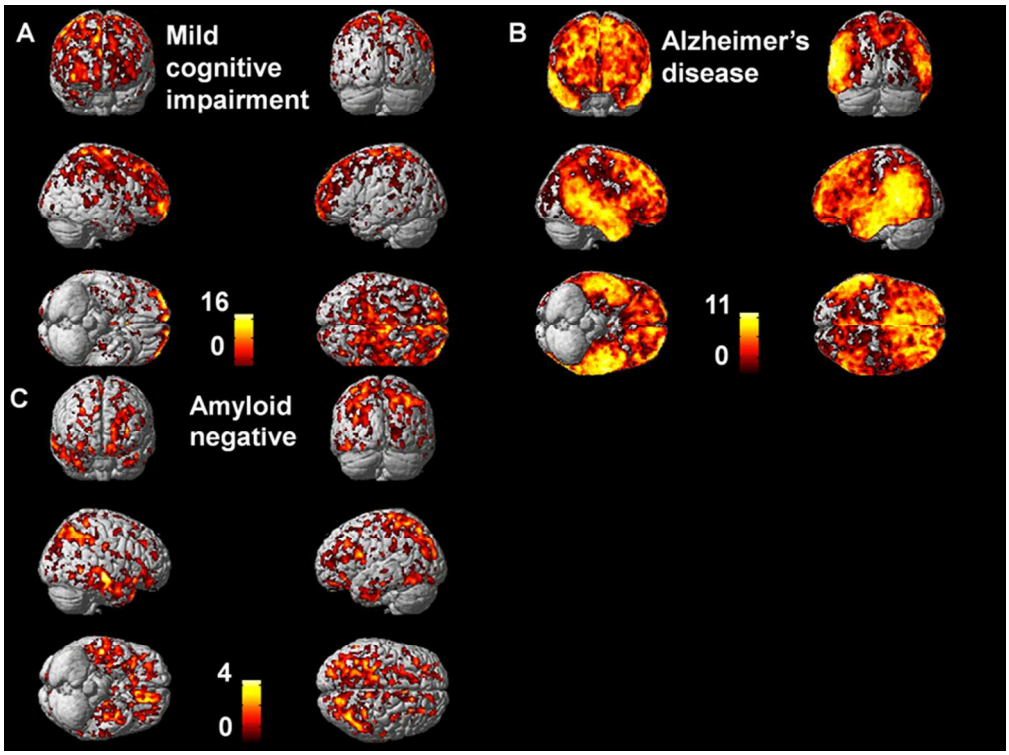

Figure 2 Voxel level correlations between tau and microglial activation in the amyloid positive mild cognitive impairment (Fig 2A), Alzheimer's disease (Fig 2B) and amyloid negative cognitively impaired individuals (Fig 2C)

90x67mm (300 x 300 DPI)

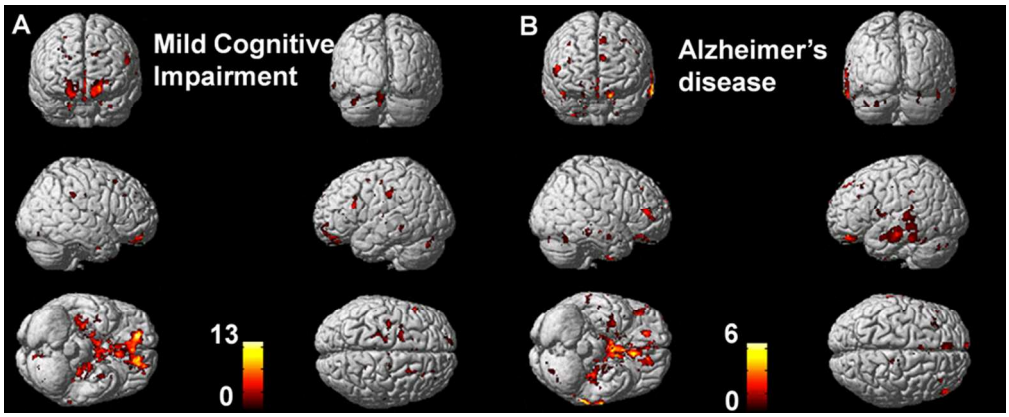

Figure 3 Voxel level correlations between amyloid and microglial activation in the amyloid positive mild cognitive impairment (Fig 3A) and Alzheimer's disease (Fig 3B) individuals

90x36mm (300 x 300 DPI)

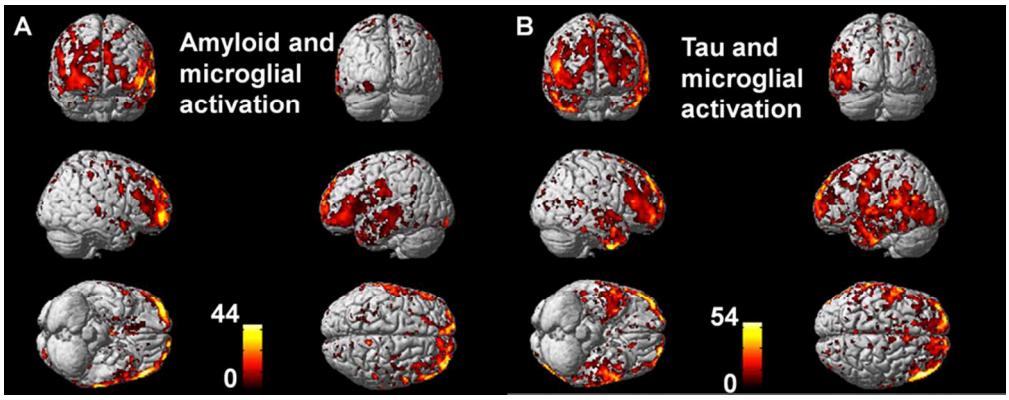

Individual levels of microglial activation correlated strongly with levels of both amyloid deposition and tau aggregation across the cortex, with Z-scores above 4 (Figure 4).

90x34mm (300 x 300 DPI)

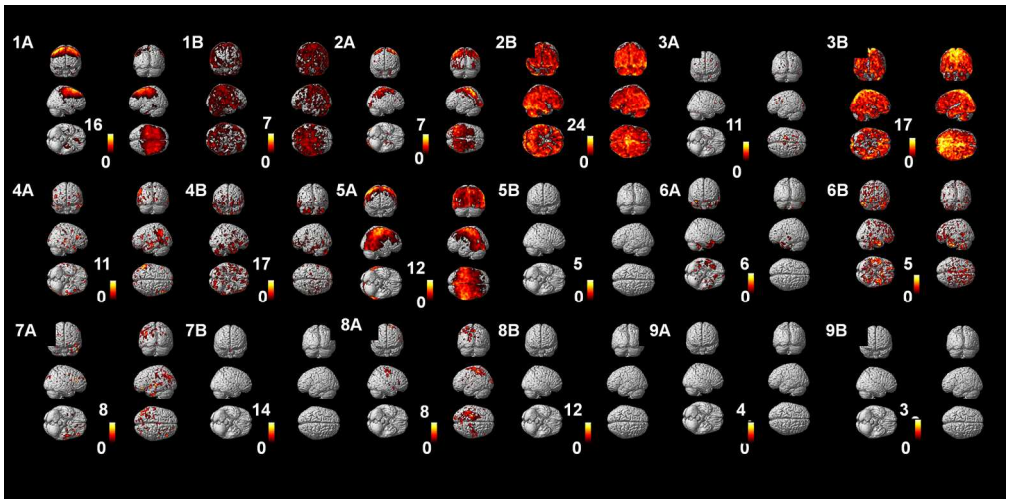

Figure 5 Individual parametric maps (Individual 1-9) of microglial activation (A) and tau aggregation (B) in the nine amyloid negative individuals with cognitive impairment, compared to the control mean. Clusters show trends of increased binding. Individuals 1,2,4,5 and 6 had statistically significant clusters of 18F-AV1451 binding, while individuals 1,2,3,4 and 6 had statistically significant 11C-PBR28 binding compared to the control groups. This figure is provided to illustrate distributions of the pathologies in this small group of individuals.

184x91mm (300 x 300 DPI)

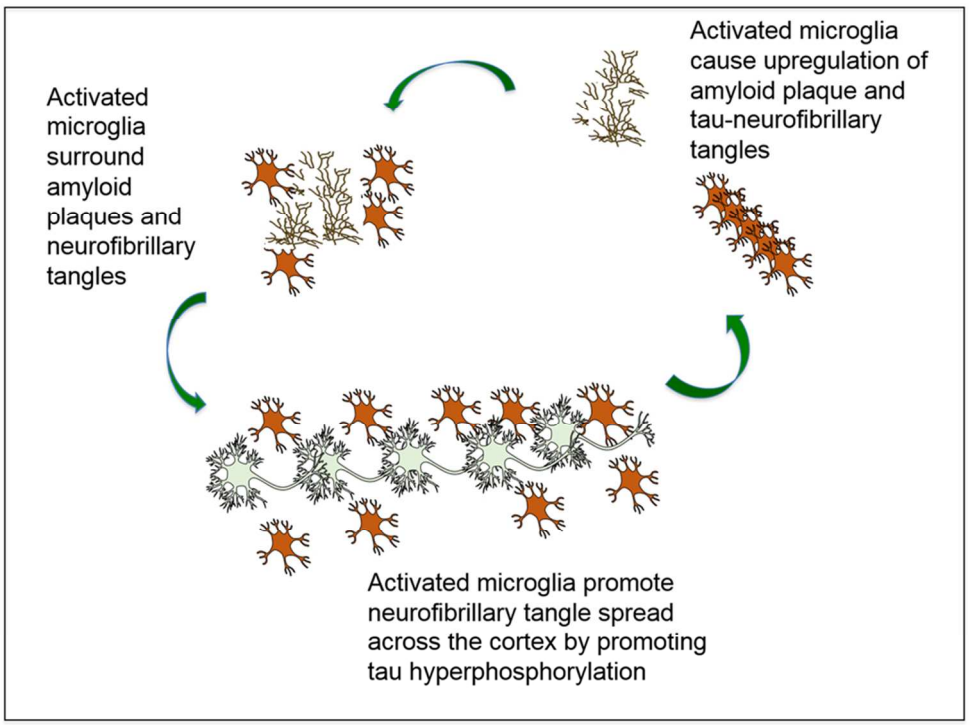

Figure 6 The vicious cycle of activated microglia and protein aggregation. Activated microglia surround amyloid plaque and neurofibrillary tangles, and in turn promote upregulation of amyloid plaque and tangles. Further, the pro-inflammatory products of activated microglia promote further tau hyperphosphorylation and spreading of neurofibrillary tangles throughout the cortex

90x66mm (300 x 300 DPI)

Supplementary Table 1 Clusters of positive correlations between ^{11}C-PBR28, ^{18}F-AV1451 and ^{18}F-flutemetamol

Region of interest	Montreal Neurological Institute Coordinates	Z-score	R correlation coefficient	p-value	Cluster size
^{18}F-AV1451 and ^{11}C-PBR28					
Mild cognitive impairment (Amyloid positive)					
Right superior frontal gyrus	5 -8 72	4.49	0.990	<0.00001	49058
Left superior frontal gyrus	-14 51 41	3.92	0.970		
Left middle frontal gyrus	-36 61 0	3.55	0.950	<0.00001	2118
Right caudate	16 -12 21	4.51	0.990	<0.00001	13813
Corpus callosum	5 0 22	4.16	0.980		
Right middle frontal gyrus	19 23 10	3.96	0.970		
Right anterior cingulate	8 6 29	3.4	0.930		
Right superior frontal gyrus	18 31 10	3.3	0.930		
Left superior frontal gyrus	-17 29 18	3.47	0.940		
Left precentral gyrus	-19 -7 31	3.43	0.940		
Left caudate	-15 -12 22	3.28	0.920		
Right superior parietal gyrus	14 -50 18	4.51	0.990	<0.00001	8830
Right posterior temporal lobe	28 -52 4	4.22	0.980		

Left superior parietal gyrus	-22 -42 24	3.77	0.960		
Left posterior temporal lobe	-22 -52 2	4.32	0.980		
Corpus callosum	12 -45 16	4.01	0.970		
Left thalamus	-5 -19 -2	4.37	0.980	<0.00001	3493
Left fusiform gyrus	-35 -16 -39	3.36	0.930	<0.00001	1548
Right lateral orbital gyrus	39 48 -9	3.18	0.910	<0.00001	2504
Right middle frontal gyrus	22 59 -5	2.9	0.880		
Right superior frontal gyrus	25 68 4	2.77	0.860		
Left superior frontal gyrus	-13 70 -4	3.9	0.970	<0.00001	560
Left precentral gyrus	58 -2 43	3.21	0.920	<0.00001	826
Right superior frontal gyrus	10 70 -2	3.36	0.930	<0.00001	1086
Right medial orbital gyrus	9 64 -19	2.86	0.880		
Left inferolateral part of PL	-50 -46 53	2.75	0.860	<0.00001	574
Alzheimer's disease (Amyloid positive)					
Right superior frontal gyrus	16 42 53	4.99	0.950	<0.00001	528779
Right insula	43 3 1	4.84	0.940		
Right anterior temporal lobe lateral part	62 3 -21	4.76	0.940		

Right anterior temporal lobe medial part	37 0 -48	4.73	0.940		
Right inferior and temporal gyrus	51 -4 -41	4.89	0.950		
Left superior frontal gyrus	-9 3 47	4.85	0.940		
Left posterior temporal lobe	-55 -43 12	4.89	0.950		
Left middle frontal gyrus	-48 25 35	4.8	0.940		
Left caudate	-16 7 21	3.91	0.870	<0.00001	1337
Left middle frontal gyrus	-22 18 12	2.91	0.740		
Left insula	-25 16 10	2.62	0.690		
Right superior parietal gyrus	43 -41 63	3.73	0.860	<0.00001	4844
Right inferolateral part of parietal lobe	43 -67 49	3.33	0.810		
Right postcentral gyrus	37 -37 65	2.59	0.690		
Right lateral part of occipital lobe	42 -71 33	2.48	0.660		
Right posterior temporal lobe	23 -35 -18	3.42	0.820	<0.00001	578
Right fusiform gyrus	30 -32 -19	3.05	0.770		
Right lateral part of occipital lobe	41 -90 -3	2.67	0.700	<0.00001	680
Left amygdala	-18 -2 -19	2.82	0.730	<0.00001	890
Left anterior temporal lobe medial part	-23 16 -38	2.78	0.720		

Left parahippocampus	-13 -5 -24	2.72	0.710		
Left posterior orbital gyrus	-24 13 -25	2.38	0.640		
Left superior parietal gyrus	0 -66 43	2.66	0.700	<0.00001	575
Right superior parietal gyrus	5 -76 42	2.63	0.690		
Amyloid negative individuals					
Right superior parietal gyrus	33 -41 61	3.41	0.940	0.003	1538
Left posterior temporal lobe	-46 -63 -16	3.4	0.930	<0.00001	3149
Left lateral part of occipital lobe	-42 -72 -14	2.72	0.860		
left superior frontal gyrus	11 48 34	2.57	0.830	0.031	1168
^{11}C-PBR28 and ^{18}F-flutemetamol					
Mild cognitive impairment (Amyloid positive)					
Right middle frontal gyrus	15 44 -9	4.23	0.980	<0.00001	36790
Right superior frontal gyrus	16 44 0	4	0.970		
Corpus callosum	8 29 -1	3.67	0.950		
Right thalamus	3 -4 4	3.61	0.950		
Right pre-subgenual frontal cortex	6 32 -3	3.59	0.950		
Right anterior orbital gyrus	17 46 -14	3.46	0.940		
Right parahippocampus	19 -10 -36	3.28	0.920		
Left pre-subgenual frontal cortex	-2 37 -7	3.83	0.960		
Left superior frontal gyrus	-13 46 -2	3.82	0.960		

Left straight gyrus	-3 21 -18	3.4	0.930		
Left anterior cingulate	-9 43 -2	3.19	0.920		
Left medial orbital gyrus	-14 45 -16	3.16	0.910		
Left middle frontal gyrus	-19 38 1	3.14	0.910		
Left anterior orbital gyrus	-16 47 -12	3.11	0.910		
Left parahippocampus	-25 -14 -26	3.95	0.970	<0.00001	7541
Left posterior temporal lobe	-27 -53 -17	3.44	0.940		
Left thalamus	-20 -29 2	3.37	0.930		
Left insula	-26 -24 7	2.92	0.890		
Left caudate	-17 8 12	2.78	0.870		
Left fusiform	-33 -18 -29	2.23	0.770		
Left amygdala	-20 -5 -18	2.15	0.750		
Right lateral part of occipital lobe	12 -98 -1	3.75	0.960	<0.00001	2126
Right cuneus	10 -95 8	2.74	0.860		
Left cuneus	-2 -98 0	1.73	0.640		
Right posterior temporal lobe	71 -44 -5	2.38	0.800	<0.00001	778
Alzheimer's disease (Amyloid positive)					
Left superior parietal gyrus	-12 -67 64	3.64	0.850	<0.00001	20616
Left inferolateral part of parietal lobe	-37 -69 51	3.36	0.810		
Left lateral part of occipital lobe	-28 -83 23	3.08	0.770		
Right precentral gyrus	32 -10 63	4.28	0.910	<0.00001	829
Right lateral part of occipital lobe	50 -65 8	3.4	0.820		

Right posterior temporal lobe	63 -52 -11	2.88	0.740		
Right inferolateral part of parietal lobe	47 -56 30	2.79	0.720		
Right posterior temporal lobe	53 -60 13	3.49	0.830	<0.00001	9206
Right lateral part of occipital lobe	50 -65 8	3.4	0.820		
Right inferolateral part of parietal lobe	47 -56 30	2.79	0.720		
Right superior parietal gyrus	12 -43 63	3.44	0.820	<0.00001	11745
Right postcentral gyrus	9 -32 58	3.44	0.820		
Right lateral part of occipital lobe	22 -69 36	3.03	0.760		
Right precentral gyrus	16 -21 63	2.89	0.740		
Left superior parietal gyrus	-1 -50 55	3.1	0.770		
Left postcentral gyrus	-1 -39 57	2.86	0.730		
Left postcentral gyrus	-40 -25 56	3.42	0.820	<0.00001	686
Left precentral gyrus	-33 -27 60	2.83	0.730		
Left precentral gyrus	-57 7 32	2.96	0.750	<0.00001	729
Left middle frontal gyrus	-48 15 42	2.45	0.660		
Right lateral part of	47 -77 25	2.03	0.570	<0.00001	713

occipital lobe					
Left inferolateral part of parietal lobe	-54 -56 21	2.75	0.720	<0.00001	629
Left lateral part of occipital lobe	-41 -71 17	2.01	0.560		
Left superior frontal gyrus	-16 -11 63	2.72	0.710	<0.00001	590
Left middle frontal gyrus	-29 0 61	2.31	0.630		
Left precentral gyrus	-20 -16 62	2	0.560		
Right lateral part of occipital lobe	26 -85 -19	2.07	0.580	<0.00001	509
Left superior parietal gyrus	-34 -47 52	2.59	0.690	<0.00001	1276
Left inferolateral part of parietal lobe	-38 -45 45	2.32	0.630		

Region	Coordinates	Z-score	R correlation coefficient	p-value	Cluster size
^{18}F-flutemetamol and ^{11}C-PBR28					
Left precentral gyrus	-57 -9 42	4.12	1.000	<0.00001	32243
Left inferior frontal gyrus	-47 39 -1	4.02	1.000		
Left middle frontal gyrus	-28 64 9	3.79	1.000		
Right lateral orbital gyrus	42 54 -16	3.77	1.000		
Left superior frontal gyrus	-21 33 56	3.68	1.000		
Right middle frontal gyrus	32 51 31	3.66	1.000		
Left superior temporal gyrus posterior part	-68 -19 -2	3.56	1.000		
Left lateral orbital gyrus	-49 44 -16	3.37	0.990		
Left middle and inferior temporal gyrus	066 017 027	3.1	0.990		
Right inferior frontal gyrus	58 27 24	3.03	0.980		
Left superior temporal gyrus posterior part	063 07 04	3.03	0.980		
Right middle frontal gyrus	38 57 3	3	0.980		
Right lateral orbital gyrus	40 50 -19	2.99	0.980		
Corpus callosum	-10 30 5	3.84	1.000	<0.00001	6635
Right caudate	18 2- 13	3.59	1.000		
Right middle frontal	18 25 11	3.57	1.000		

gyrus					
Right subgenual frontal cortex	2 22 -6	3.27	0.990		
Right insula	21 26	3	0.980		
Left anterior temporal lobe medial part	-34 19 -39	3.19	0.990	0.032	1323
Left anterior temporal lobe lateral part	-53 12 -29	2.75	0.970		
Left superior temporal gyrus anterior part	-45 22 -27	2.52	0.950		
Left middle and inferior temporal gyrus	-58 -2 -35	2.18	0.910		
Right posterior temporal lobe	19 -36 5	3.03	0.980	0.011	1526
Corpus callosum	15 -27 25	2.59	0.960		
Right superior parietal gyrus	19 -30 29	2.56	0.960		
Corpus callosum	-12 -17 29	2.98	0.980	<0.00001	2481
Left postcentral gyrus	-16 -18 31	2.64	0.960		
Left posterior cingulate cortex	-9 -36 27	2.28	0.930		
Left precentral gyrus	-57 -9 42	3.12	1.000	0.021	149
Left postcentral gyrus	-60 -14 37	2.92	0.980		
Left inferior frontal gyrus	-47 39 -1	4.02	1.000	<0.00001	1249
Left lateral orbital gyrus	-49 44 -16	3.37	0.990		
Left middle frontal gyrus	-48 49 -10	3.11	0.990		
Right thalamus	2 -12 3	3.81	1.000	<0.00001	602
Left middle frontal gyrus	-28 64 9	3.79	1.000	0.001	205

Right medial orbital gyrus	42 54 -16	3.77	1.000	<0.00001	1704
Right middle frontal gyrus	38 57 3	3	0.980		
Right anterior orbital gyrus	31 59 -7	2.67	0.970		
Right middle frontal gyrus	32 51 31	3.66	1.000	0.022	148
Right caudate	18 20 13	3.59	1.000	<0.00001	295
Right middle frontal gyrus	18 26 11	3.57	1.000		
Right insula	21 26 4	3	0.980		
Corpus callosum	16 30 6	2.94	0.980		
Left superior frontal gyrus	-12 69 4	3.57	1.000	<0.00001	689
Left superior temporal gyrus posterior part	-68 -19 -2	3.56	1.000	<0.00001	739
Left middle and inferior temporal gyrus	-66 -17 -27	3.13	0.990		
Corpus callosum	0 25 -2	3.3	0.990	0.026	145
Right subgenual frontal cortex	2 22 -6	3.27	0.990		
^{18}F-AV1451 and ^{11}C-PBR28					
Right middle frontal gyrus	52 39 17	4.25	1.000	<0.00001	15651
Right superior frontal gyrus	13 68 13	3.99	1.000		
Right inferior frontal gyrus	51 36 12	3.82	1.000		
Right anterior orbital gyrus	25 65 -7	3.41	0.990		
Right lateral orbital	41 56 -7	2.93	0.980		

gyrus					
Right posterior temporal lobe	40 -50 4	3.75	1.000	<0.00001	2189
Left superior frontal gyrus	-17 25 62	3.63	1.000	<0.00001	10412
Left middle frontal gyrus	-46 48 15	3.07	0.990		
Left anterior orbital gyrus	-23 65 -7	2.6	0.960		
Right superior frontal gyrus	2 17 64	3.08	0.990	0.004	1592
Left superior frontal gyrus	-2 11 54	2.83	0.980		
Left inferolateral part of parietal lobe	-32 -44 37	4.1	1.000	<0.00001	218
Left superior parietal gyrus	-25 -44 39	3.33	0.990		
Right superior frontal gyrus	13 68 13	3.99	1.000	<0.00001	563
Right anterior orbital gyrus	25 65 -7	3.41	0.990		
Left posterior temporal lobe	-49 -46 5	3.99	1.000	<0.00001	463
Left middle and inferior temporal gyrus	-50 -8 -39	3.99	1.000	<0.00001	727
Left anterior temporal lobe lateral part	-54 0 -39	2.92	0.980		
Right lateral occipital lobe	29 -73 11	3.88	1.000	<0.00001	245
Right middle frontal gyrus	52 39 17	4.25	1.000	<0.00001	1257
Right inferior frontal	51 36 12	3.82	1.000		

gyrus					
Left inferolateral part of parietal lobe	-32 -44 37	4.1	1.000	<0.00001	218
Left superior parietal gyrus	-25 -44 39	3.33	0.990		
Right superior frontal gyrus	13 68 13	3.99	1.000	<0.00001	563
Right anterior orbital gyrus	25 65-7	3.41	0.990		
Left posterior temporal lobe	-49 -46 5	3.99	1.000	<0.00001	463
Left middle and inferior and temporal gyrus	-50 -8 -39	3.99	1.000	<0.00001	727
Left anterior temporal lobe lateral part	-54 0 -39	2.92	0.980		
Right lateral occipital lobe	29 -73 11	3.88	1.000	<0.00001	245
Left superior temporal gyrus posterior part	-52 -1 0	3.86	1.000	<0.00001	525
Left precentral gyrus	-61 4 15	3.84	1.000		
Right anterior temporal lobe medial part	28 7 -30	3.79	1.000	0.007	156
Left superior temporal gyrus posterior part	-49 -9-1	3.74	1.000	<0.00001	229
Right anterior temporal lobe medial part	27 1 -47	3.68	1.000	<0.00001	256
Right fusiform	32 -5 -45	2.52	0.950		
Left posterior temporal lobe	-41 -42 -20	3.65	1.000	<0.00001	661
Right superior parietal	15 -44 26	3.64	1.000	<0.00001	1325

gyrus					
Corpus callosum	19 -43 20	3.32	0.990		
Left anterior temporal lobe lateral part	-56 4 -27	3.63	1.000	<0.00001	249
Left lateral part of occipital lobe	-50 -77 -9	3.62	1.000	<0.00001	843
Right middle frontal gyrus	39 56 -1	3.55	1.000	<0.00001	836
Right inferior frontal gyrus	53 42 -1	3.29	0.990		
Right lateral orbital gyrus	41 56 -7	2.93	0.980		
Left superior temporal gyrus posterior part	-37 -32 -8	3.5	0.990	0.007	156
Left middle and inferior temporal gyrus	-40 -32 -11	3.42	0.990		
Left superior frontal gyrus	-18 58 34	3.5	0.990	0.002	179
Left precentral gyrus	-60 2 37	3.44	0.990	<0.00001	477
Left superior frontal gyrus	-14 67 17	3.32	0.990	<0.00001	720

Supplementary table 2 - Voxel level comparisons between the tracer positive individuals and healthy controls for each tracer

^{11}C-PBR28 High affinity binders				
Region	**Coordinates**	**Z-score**	**p-value**	**Cluster size**
Left middle and inferior temporal gyrus	-44 -3 -32	4.69	<0.00001	1024962
Right fusiform gyrus	32 -9 -38	4.63		
Left postcentral gyrus	-16 -31 59	4.54		
Right middle and inferior temporal gyrus	56 -28 -25	4.36		
Left posterior temporal lobe	-49 -45 -9	4.28		
Right amygdala	29 -5 -26	4.28		
Right superior parietal gyrus	24 -6038	4.27		
Left middle frontal gyrus	-26 0 46	4.22		
Left lateral part of occipital lobe	-28 -71 27	4.22		
Left superior parietal gyrus	-21 -41 50	4.21		
Left postcentral gyrus	-30 -31 48	4.2		
Left amygdala	-23 -5 -29	4.18		
Left precentral gyrus	-36 -12 34	4.17		
Right fusiform gyrus	32 -9 -38	4.63	0.003	1204
Right anterior temporal lobe lateral part	43 3 -37	4.16		
Right anterior temporal lobe medial part	27 2 -41	3.8		
Right middle and inferior temporal gyrus	36 -3 -41	3.66		
Left postcentral gyrus	-16 -31 59	4.54	<0.00001	37439
Left posterior temporal	-49 -45 -9	4.28		

lobe				
Left lateral part of occipital lobe	-28 -71 27	4.22		
Left superior parietal gyrus	-21 -41 50	4.21		
Right postcentral gyrus	34 -27 38	4.05		
Right superior parietal gyrus	24 -60 38	4.27	<0.00001	3318
Right inferolateral part of parietal lobe	33 -49 36	4.02		
Left middle frontal gyrus	-26 0 46	4.22	<0.00001	3556
Left precentral gyrus	-36 -12 34	4.17		
Left superior frontal gyrus	-19 7 43	3.37		
Right precentral gyrus	14 -21 55	4.16	<0.00001	7260
Right superior frontal gyrus	8 -29 54	3.86		
Right middle frontal gyrus	30 11 38	3.78		
Right precentral gyrus	18 -23 60	3.6		
Left middle inferior temporal gyrus	-51 -27 -27	4.14	<0.00001	1750
Right middle and inferior temporal gyrus	-52 -20 -23	3.9		
Left fusiform gyrus	-41 -27 -23	3.4		
Left medial orbital gyrus	-18 29 -18	3.94	<0.00001	2322
Left posterior orbital gyrus	-33 30 -7	3.85		
Left insula	-29 27 -3	3.65		
Left putamen	-19 15 -10	3.56		
Left nucleus accumbens	-12 12 -9	3.37		
Left inferior frontal gyrus	-44 34 -5	3.29		
Left middle frontal gyrus	-23 24 -6	3.21		
Right lateral part of occipital lobe	35 -83 -14	3.77	0.013	958

Left postcentral gyrus	-45 -25 37	3.76	0.009	1012
Left inferolateral part of parietal lobe	-52 -23 27	3.62		
Left lingual gyrus	-15 -78 -6	3.74		
Left lateral part of occipital lobe	-17 -83 -13	3.45		
Right inferior frontal gyrus	41 7 14	3.68	0.03	821
Right insula	33 11 9	3.31		
^{18}F-flutemetamol				
Corpus callosum	2 -36 15	6.77	<0.00001	1031605
Left posterior orbital gyrus	-23 27 -23	6.7		
Right anterior cingulate cortex	3 39 18	6.37		
Left medial orbital gyrus	-13 28 -26	6.32		
Left superior frontal gyrus	-3 36 35	6.26		
Right superior frontal gyrus	2 51 9	6.21		
Left superior temporal gyrus anterior part	-47 19 -20	6.2		
Left posterior cingulate cortex	0 -20 28	6.2		
Right posterior orbital gyrus	22 29 -24	6.17		
Right middle and inferior temporal gyrus	60 -18 -18	6.16		
^{18}F-AV1451				
Corpus callosum	-1 -17 26	5.13	<0.00001	997291
Right anterior temporal gyrus, medial part	23 8 -49	4.88		
Right superior parietal gyrus	1 -42 39	4.73		

Left anterior temporal gyrus medial part	-22 6 -44	4.71

Region of interest	Montreal Neurological Institute Coordinates	Z-score	R correlation coefficient	Cluster size	p-value
^{18}F-flutemetamol and ^{11}C-PBR28 - mild cognitive impairment individuals					
Right superior frontal gyrus	13 46 -7	5	0.990	40707	<0.00001
Right caudate	14 3 21	4.14	0.990		
Left anterior cingulate cortex	-9 44 0	4.05	0.970		
Left superior frontal gyrus	-13 46 1	4.03	0.970		
Right thalamus	18 -23 10	3.63	0.950		
Right pre-subgenual frontal cortex	2 34 -3	3.51	0.940		
Right pallidum	17 -3-4	3.47	0.940		
Left thalamus	-13 -15 1	3.42	0.940		
Left medial orbital gyrus	4 52 -12	3.36	0.930		
Left middle frontal gyrus	-19 31 14	3.35	0.930		
Left superior frontal gyrus	-17 37 12	3.31	0.930		
Left pre-subgenual frontal cortex	-3 42 -4	3.3	0.930		
Right caudate	20 -18 21	3.26	0.920		
Corpus callosum	2 28 12	3.26	0.920		
Right straight gyrus	6 34 -18	3.25	0.920		
Left anterior cingulate cortex	-4 33 12	3.21	0.920		
Left substantia nigra	-11 -21 -13	4.12	0.980	<0.00001	5142
Left posterior temporal lobe	-27 -54 -17	3.73	0.960		
Left hippocampus	-30 -33 -9	3.16	0.910		
Left posterior temporal lobe	-25 -36 -2	3.08	0.900		

Left parahippocampus	-21 -28 -16	2.95	0.890		
Left superior temporal gyrus, posterior part	-36 -29 3	2.93	0.890		
Left posterior temporal lobe	-27 -35 -6	2.91	0.880		
Left lingual	-26 -54 -11	2.90	0.880		
Left insula	-28 -28 12	2.90	0.880		
Left fusiform gyrus	-38 -34 -16	2.68	0.850		
Left insula	-33 -26 3	2.6	0.840		
Right inferior frontal gyrus	-33 -28 9	2.49	0.820		
Left thalamus	-16 -26 4	2.29	0.780		
Left superior temporal gyrus posterior part	-37 -28 -1	2.21	0.760		
Left precentral gyrus	-18 -23 58	3.48	0.940		
Left postcentral gyrus	-13 -33 53	3.46	0.940		
Right superior frontal gyrus	13 46 -7	5	0.990	<0.00001	1083
Right medial orbital gyrus	4 52 -12	3.36	0.930		
Right anterior cingulate cortex	12 41 3	3.08	0.900		
Right middle frontal gyrus	17 47 -6	2.68	0.850		
Right anterior orbital gyrus	16 54 -16	2.51	0.820		
Right thalamus	3 -7 3	3.5	0.940	<0.00001	1966
Right pallidum	17 -3 -4	3.47	0.940		
Right caudate	9 6 10	3.02	0.900		
Left thalamus	-3 -9 2	2.99	0.890		
Left anterior cingulate cortex	-9 44 0	4.05	0.970	<0.00001	3353
Left superior frontal	-13 46 1	4.03	0.970		

gyrus					
Right pre-subgenual frontal cortex	2 34 -3	3.51	0.940		
Right superior frontal gyrus	5 45 -10	3.43	0.940		
Left middle frontal gyrus	-19 31 14	3.35	0.930		
Left pre-subgenual frontal cortex	-3 42 -4	3.3	0.930		
Right straight gyrus	6 34 -18	3.25	0.92		
Corpus callosum	-13 34 3	3.17	0.910		
Right anterior cingulate cortex	2 42 6	3.08	0.900		
Left middle frontal gyrus	-22 34 11	3.04	0.900		
Left superior frontal gyrus	5 42 -7	2.94	0.890		
Left medial orbital gyrus	-10 52 -15	2.86	0.880		
Left anterior orbital gyrus	-20 48 -10	2.82	0.870		
Left middle frontal gyrus	-19 27 16	2.77	0.860		
Left anterior cingulate cortex	-7 36 9	2.58	0.830		
^{18}F-flutemetamol and ^{11}C-PBR28– Alzheimer's disease subjects					
Right middle frontal gyrus	21 35 0	3.95	0.880	<0.00001	26656
Left thalamus	-21 -26 -6	3.9	0.870		
Right straight gyrus	3 43 -21	3.64	0.850		
Right superior frontal gyrus	3 43 -10	3.64	0.850		
Left caudate	-15 8 12	3.43	0.820		
Right caudate	14 15 11	3.39	0.810		
Right middle frontal gyrus	20 38 03	3.36	0.810		
Right anterior orbital	21 43 -8	3.32	0.800		

gyrus					
Left medial orbital gyrus	-9 45 -21	3.31	0.800		
Right insula	32 -27 -2	3.15	0.780		
Left fusiform	-39 -27 -25	3.1	0.770		
Right putamen	26 -9 7	3.1	0.770		
Left superior frontal gyrus	-1 44 -12	3.08	0.770		
Left pallidum	-15 5 -2	2.96	0.750		
^{18}F-AV1451 and ^{11}C-PBR28 – mild cognitive impairment subjects					
Right superior frontal gyrus	13 41 39	4.54	0.990	1691	<0.00001
Right posterior temporal lobe	31 -57 4	4.54	0.990	135987	<0.00001
Left superior frontal gyrus	-3 -13 69	4.5	0.990		
Left superior parietal gyrus	-40 -43 63	4.49	0.990		
Right superior frontal gyrus	5 63 29	4.47	0.990		
Left middle frontal gyrus	-43 56 -3	4.46	0.990		
Right precentral gyrus	4 -15 56	4.4	0.980		
Right postcentral gyrus	25 -18 35	4.3	0.980		
Right posterior temporal lobe	27 -56 4	4.29	0.980		
Left precentral gyrus	-3 -32 69	4.27	0.980		
Corpus callosum	-9 25 7	4.23	0.980		
Right caudate	14 21 -1	4.22	0.980		
Right precentral gyrus	6 -15 75	4.19	0.980		
Left superior parietal gyrus	-27 -57 66	4.19	0.980		
Right superior parietal gyrus	25 -45 73	4.11	0.970		
Left anterior cingulate	0 6 39	4.08	0.970		

cortex					
Right superior frontal gyrus	3 -3 65	4.01	0.970		
Right postcentral gyrus	4 -30 57	4	0.970		
Left superior frontal gyrus	-1 -5 55	4	0.970		
Right posterior cingulate cortex	2 -25 27	3.98	0.970		
Right anterior orbital gyrus	28 66 -8	3.94	0.970		
Left middle frontal gyrus	-38 61 0	3.94	0.970		
Left lateral remainder of occipital lobe	-27 -72 0	3.92	0.970		
Right postcentral gyrus	50 -15 34	3.9	0.970		
Right posterior temporal lobe	23 -48 8	3.87	0.960		
Right lateral remainder of occipital lobe	31 -61 3	3.86	0.960		
Left lateral remainder of occipital lobe	-5 -101 -2	4.06	0.970	<0.00001	2561
Left cuneus	-7 -100 19	3.14	0.910		
Left lingual	-3 -98 -5	2.52	0.820		
Left lateral remainder of occipital lobe	-32 -90 14	1.92	0.690		
Right anterior temporal lobe medial part	35 9 -28	3.59	0.950	<0.00001	2213
Right anterior temporal lobe lateral part	43 21 -37	3.56	0.950		
Right superior temporal gyrus anterior part	42 24 -33	2.82	0.870		
Right fusiform gyrus	37 -31 -29	3.57	0.950	<0.00001	1155
Right hippocampus	26 -18 -14	3.01	0.900		
Right amygdala	24 -9 -12	2.83	0.870		

Right parahippocampus	23 -24 -16	2.65	0.850		
Right middle and inferior temporal gyrus	41 -14 -20	2.29	0.780		
Right posterior temporal lobe	41 -34 -29	2.26	0.780		
Right insula	35 -7 -17	1.76	0.650		
Left precentral gyrus	-55 0 39	3.26	0.920	0.004	798
Left middle frontal gyrus	-50 2 52	2.15	0.750		
Right lateral remainder of occipital lobe	31 -76 49	3.19	0.920	0.001	949
Right inferolateral remainder of parietal lobe	41 -71 43	2.86	0.880		
Right superior temporal gyrus anterior part	52 14 -7	3.05	0.900	<0.0001	1118
Right middle and inferior temporal gyrus	64 1 -15	2.78	0.870		
Right superior temporal gyrus posterior part	57 0 -16	2.28	0.780		
Right anterior temporal lobe lateral part	60 8 -26	2.01	0.720		
Left middle frontal gyrus	-38 54 22	2.84	0.870	0.019	674
Right amygdala	16 0 -28	2.5	0.820	0.042	609
Right fusiform gyrus	27 -13 -39	2.29	0.780		
Right parahippocampus	22 -12 -35	2.2	0.760		
Right superior frontal gyrus	13 41 39	4.54	0.990	<0.00001	649
Right posterior temporal lobe	31 -57 4	4.54	0.990	<0.00001	1729
Right lateral remainder of occipital lobe	31 -61 3	3.86	0.960		
Right superior parietal gyrus	18 -49 16	3.45	0.940		

Right lingual gyrus	26 -62 1	2.54	0.830		
Left superior frontal gyrus	-3 -13 69	4.5	0.990	<0.00001	1457
Right precentral gyrus	4 -15 56	4.4	0.980		
Right superior frontal gyrus	3 -3 65	4.01	0.970		
Left superior parietal gyrus	-40 -43 63	4.49	0.990	<0.00001	665
Left postcentral gyrus	-48 -36 60	3.42	0.940		
Left inferolateral remainder of parietal lobe	-49 -40 56	2.69	0.850		
Right superior frontal gyrus	5 63 29	4.47	0.990	<0.00001	755
Left superior frontal gyrus	0 52 23	3.54	0.950		
Left precentral gyrus	-3 -32 69	4.27	0.980	<0.00001	1523
Left postcentral gyrus	-17 -33 73	3.77	0.960		
Left superior parietal gyrus	-17 -41 66	3.29	0.920		
Corpus callosum	-9 25 7	4.23	0.980	<0.00001	4468
Left lateral remainder of occipital lobe	-27 -72 0	3.92	0.970		
Left middle frontal gyrus	-21 4 26	3.69	0.950		
Left inferolateral remainder of parietal lobe	-28 -22 25	3.65	0.950		
Left precentral gyrus	-27 -11 29	3.56	0.950		
Left posterior temporal lobe	-28 -54 2	3.51	0.940		
Left insula	-22 -24 18	3.39	0.930		
Left superior frontal gyrus	-13 24 24	3.23	0.920		

Left lateral remainder of occipital lobe	-29 -68 -4	3.13	0.910		
Left caudate	-18 -20 24	3.1	0.910		
Left postcentral gyrus	-32 -17 33	3.05	0.900		
Left middle frontal gyrus	-18 6 24	3.01	0.900		
Left posterior temporal lobe	-27 -61 4	2.98	0.890		
Right caudate	14 21 -1	4.22	0.980	<0.00001	1999
Corpus callosum	17 30 9	3.18	0.910		
Right middle frontal gyrus	20 15 21	3.14	0.910		
Right subgenual frontal cortex	1 21 -4	3.13	0.910		
Right subcallosal area	1 14 -10	2.41	0.810		
Left anterior cingulate cortex	0 6 39	4.08	0.970	<0.00001	753
Left superior frontal gyrus	-1 -5 55	4	0.970		
Right posterior cingulate cortex	2 -25 27	3.98	0.970	<0.00001	637
Corpus callosum	2 -31 18	3.71	0.960		
Left posterior cingulate cortex	-4 -28 28	3.01	0.900		
Right anterior orbital gyrus	28 66 -8	3.94	0.970	<0.00001	819
Right middle frontal gyrus	29 65 -4	3.51	0.940		
Right caudate	20 -18 21	3.83	0.960	<0.00001	948
Right postcentral gyrus	25 -18 24	3.42	0.940		
Right inferolateral remainder of parietal lobe	23 -24 24	3.42	0.940		
Right thalamus	12 -7 16	3.26	0.920		

Corpus callosum	-5 -13 24	2.81	0.870		
Corpus callosum	4 4 25	3.67	0.950	<0.00001	765
Right anterior cingulate	11 3 33	2.68	0.850		
Right precentral gyrus	31 -24 66	3.47	0.940	<0.00001	586
Right postcentral gyrus	43 -20 -56	3.23	0.920		
Tau and microglial activation – Alzheimer's disease subjects					
Right middle frontal gyrus	35 57 19	5.57	0.970	<0.00001	253556
Right inferolateral part of parietal lobe	64 -26 46	5.17	0.960		
Left anterior temporal lobe lateral part	-60 4 -22	5.09	0.960		
Right anterior temporal lobe lateral part	58 4 -27	5.08	0.960		
Left superior frontal gyrus	-21 69 2	4.93	0.950		
Right superior frontal gyrus	25 63 24	4.93	0.950		
Right postcentral gyrus	56 -17 55	4.69	0.940		
Left middle frontal gyrus	-40 53 17	4.66	0.930		
Left posterior temporal lobe	-55 -47 14	4.64	0.930		
Right superior temporal gyrus anterior part	53 13 -20	4.64	0.930		
Right superior temporal gyrus posterior part	65 2 -4	4.59	0.930		
Left precentral gyrus	-46 -6 12	4.48	0.920		
Right posterior temporal lobe	35 -51 -6	4.47	0.920		
Left middle and inferior temporal gyrus	-42 -4 -46	4.46	0.920		
Left inferolateral remainder of parietal	-68 -37 31	4.41	0.920		

lobe					
Left superior parietal gyrus	-2 -62 56	4.35	0.910	<0.00001	5272
Right superior parietal gyrus	6 -72 36	3.69	0.850		
Left postcentral gyrus	-10 -39 77	3.15	0.780		
Left parahippocampus	-25 -29 -22	3.41	0.820	0.001	595
Left posterior temporal lobe	-30 -41 -18	3.1	0.770		
Left inferolateral part of parietal lobe	-30 -61 30	3.22	0.790	0.003	502
Left superior parietal gyrus	-25 -59 33	2.72	0.710	0.003	501
Right middle frontal gyrus	35 57 19	5.57	0.970	<0.00001	1506
Right superior frontal gyrus	25 63 24	4.93	0.950		
Left anterior temporal lobe lateral part	-60 4 -22	5.09	0.960	<0.00001	4049
Left middle and inferior temporal gyrus	-42 -4 -46	4.46	0.920		
Left superior temporal gyrus posterior part	-54 17 -8	3.73	0.860		
Right anterior temporal lobe lateral part	58 4 -27	5.08	0.960	<0.00001	1467
Right superior temporal gyrus posterior part	65 2 -4	4.59	0.930		
Left superior frontal gyrus	-21 69 2	4.93	0.950	<0.00001	1669
Left middle frontal gyrus	-40 53 17	4.66	0.930		
Left anterior orbital gyrus	-28 65 -12	3.58	0.840		
Left posterior temporal	-55 -47 14	4.64	0.930	<0.00001	8212

lobe					
Left inferolateral part of parietal lobe	-68 -37 31	4.41	0.920		
Left superior temporal gyrus posterior part	-58 -24 10	4.29	0.910		
Left middle and inferior temporal gyrus	-70 -30 -4	3.71	0.850		
Left superior frontal gyrus	-13 -2 62	4.5	0.920	<0.00001	1970
Left precentral gyrus	-46 -6 12	4.48	0.920	<0.00001	669
Left insula	-40 -10 8	3.56	0.840		
Left postcentral gyrus	-44 -9 7	3.55	0.830		
Left superior temporal gyrus posterior part	-51 1 -2	3.52	0.830		
Right superior temporal gyrus posterior part	61 -24 3	4.45	0.920	<0.00001	7414
Right posterior temporal lobe	47 -35 3	4.37	0.910		
Right middle and inferior temporal gyrus	65 -16 -14	4.3	0.910		
Right inferolateral part of parietal lobe	52 -46 21	3.79	0.860		
Right superior parietal gyrus	18 -45 30	4.04	0.890	<0.00001	984
Corpus callosum	0 -26 26	3.98	0.880		
Right posterior cingulate cortex	3 -44 22	3.37	0.810		
Right middle frontal gyrus	27 34 21	4.03	0.890	<0.00001	551
Right middle frontal gyrus	35 57 19	5.57	0.970	<0.00001	663578
Right inferolateral part of parietal lobe	64 -26 46	5.17	0.960		

Left anterior temporal lobe lateral part	-60 4 -22	5.09	0.960		
Right anterior temporal lobe lateral part	58 4 -27	5.08	0.960		
Left superior frontal gyrus	-21 69 2	4.93	0.950		
Right superior frontal gyrus	25 63 24	4.93	0.950		
Right postcentral gyrus	56 -17 55	4.69	0.940		
Left middle frontal gyrus	-40 53 17	4.66	0.930		
Left posterior temporal lobe	-55 -47 14	4.64	0.930		
Right superior temporal gyrus anterior part	53 13 -20	4.64	0.930		
Right superior temporal gyrus posterior part	65 2 -4	4.59	0.930		
Left precentral gyrus	-46 -6 12	4.48	0.920		
Right posterior temporal lobe	35 -51 -6	4.47	0.920		
Left middle and inferior temporal gyrus	-42 -4 -46	4.46	0.920		
Left inferolateral part of parietal lobe	-54 -21 17	4.36	0.910		
^{18}F-AV1451 and ^{11}C-PBR28 - Amyloid negative individuals					
Left middle and inferior temporal gyrus	-35 -4 -26	5.1	0.990	<0.00001	125462
Left insula	-35 -2 -19	4.84	0.990		
Right anterior temporal lobe lateral art	51 4 -26	4.4	0.980		
Left posterior temporal lobe	-21 -47 1	4.36	0.980		
Left inferolateral part of parietal lobe	-37 -72 48	4.23	0.980		

Right superior temporal gyrus anterior part	51 10 -20	4.19	0.980		
Right lateral part of occipital lobe	24 -66 18	4.01	0.970		
Left thalamus	-6 -3 7	3.99	0.970		
Right fusiform gyrus	32 -17 -38	3.95	0.970		
Right inferolateral remainder of parietal lobe	34 -65 53	3.88	0.970		
Right inferior frontal gyrus	56 9 1	3.88	0.970		
Right superior parietal gyrus	10 -51 73	3.88	0.960		
Right anterior temporal lobe medial part	16 2 -31	3.86	0.960		
Left precentral gyrus	-17 -12 75	3.82	0.960		
Left fusiform gyrus	-36 -17 -22	3.82	0.960		
Left inferolateral part of parietal lobe	-42 -46 52	3.8	0.960		
Right lateral part of occipital lobe	23 -68 8	3.79	0.960		
Corpus callosum	-12 -46 14	3.77	0.960		
Left insula	-24 -28 15	3.76	0.960		
Right fusiform gyrus	28 -9 -42	3.75	0.960		
Left middle frontal gyrus	-16 45 -4	3.75	0.960		
Left postcentral gyrus	-18 -28 75	3.74	0.960		
Left inferior frontal gyrus	-53 11 20	4.89	0.990	0.001	1956
Left precentral gyrus	-45 2 15	3.35	0.930		
Left middle frontal gyrus	-49 9 44	2.34	0.790		
Right middle frontal gyrus	25 56 16	3.85	0.960	<0.00001	2352
Right superior frontal	18 63 16	2.43	0.81		

gyrus					
Right anterior temporal lobe lateral part	51 4 -26	4.4	0.980	<0.00001	3121
Right superior temporal gyrus anterior part	51 10 -20	4.19	0.980		
Right inferior frontal gyrus	56 9 1	3.88	0.970		
Right anterior temporal lobe medial part	36 12 -40	3.62	0.950		
Right middle and inferior temporal gyrus	53 -5 -19	3.58	0.950		
Right superior temporal gyrus posterior part	65 2 -7	2.93	0.890		
Left posterior temporal lobe	-21 -47 1	4.36	0.980	<0.00001	3275
Left lateral remainder of occipital lobe	-27 -73 -1	3.59	0.950		
Left lingual gyrus	-26 -65 -3	3.59	0.950		
Left middle and inferior temporal gyrus	-40 -31 -10	2.7	0.850		
Right insula	27 18 2	4.04	0.970		
Right posterior orbital gyrus	26 25 -12	4	0.970		
Right putamen	24 14 -4	2.72	0.860		
Right insula	27 18 2	4.03	0.970	<0.00001	722
Right posterior orbital gyrus	26 25 -12	4	0.970		
Right putamen	24 14 -4	2.72	0.860		
Left middle frontal gyrus	-16 45 -4	3.75	0.960	<0.00001	1630
Corpus callosum	-13 31 11	3.62	0.950		
Left anterior cingulate cortex	-5 6 33	3.44	0.940		
Left medial orbital gyrus	-5 37 -17	3.31	0.930		

Left superior frontal gyrus	-16 29 20	2.97	0.890		
Left pre-subgenual frontal cortex	-6 36 -11	2.52	0.820		
Left subgenual frontal cortex	-7 31 -10	2.44	0.810		
Left middle frontal gyrus	-15 34 -4	2.39	0.800		
Left middle frontal gyrus	-16 45 -4	3.75	0.960	<0.00001	1630
Corpus callosum	-13 31 11	3.62	0.950		
Left anterior cingulate cortex	-5 6 33	3.44	0.940		
Left medial orbital gyrus	-5 37 -17	3.31	0.930		
Left superior frontal gyrus	-16 29 20	2.97	0.890		
Left pre-subgenual frontal cortex	-6 36 -11	2.52	0.820		
Left subgenual frontal cortex	-7 31 -10	2.44	0.810		
Right lateral remainder of occipital lobe	20 -83 6	3.26	0.920	<0.00001	512
Right lingual gyrus	14 -81 6	2.75	0.860		

Subject	Region	Coordinates	Z score	p-value	Cluster size
AD1 – ^{11}C-PBR28	Left superior parietal gyrus	-27 -39 48	3.35	<0.00001	24158
	Left posterior temporal lobe	-47 -51 5	3.09		
	Left lateral remainder of occipital lobe	-29 -82 15	3.08		
	Left postcentral gyrus	-26 -35 47	3.02		
AD1 – ^{18}F-AV1451	Right superior parietal gyrus	2 -51 16	6.31	<0.00001	776294
	Right posterior temporal lobe	49 -60 2	6.29		
	Right lateral part of occipital lobe	37 -73 -19	5.92		
	Left middle and inferior temporal gyrus	-63 -13 -26	5.87		
	Corpus callosum	5 -42 11	5.82		
AD2 – ^{11}C PBR28	Right superior parietal gyrus	18 -45 -40	4.28	<0.00001	681404
	Right posterior temporal lobe	36 -58 8	4.2		
	Left middle frontal gyrus	-25 33 13	4.12		
	Left superior parietal gyrus	-16 -52 44	4.05		
	Right lateral remainder of occipital lobe	41 -63 9	3.99		
	Left inferolateral remainder o parietal lobe	-47 -50 34	3.99		
	Right precentral gyrus	23 -22 46	3.92		
	Right superior frontal gyrus	17 -6 51	3.91		
	Right middle and inferior temporal gyrus	36 -7 -43	3.89		
	Right inferolateral remainder of parietal lobe	49 -44 32	3.89		

	Left superior parietal gyrus	-10 -46 35	3.87		
	Left lingual gyrus	-11 -47 -3	3.86		
AD2 – ^{18}F-AV1451	Left posterior temporal lobe	-51 -44 7	6.01	<0.00001	572923
	Left middle and inferior frontal gyrus	-64 -24 -6	5.86		
	Left posterior cingulate cortex	-2 -40 25	5.85		
	Left superior temporal gyrus posterior part	-64 -28 5	5.81		
	Right posterior temporal lobe	54 -37 -4	5.78		
	Right superior parietal gyrus	2 -50 17	5.76		
	Right middle and inferior temporal gyrus	66 -20 -21	5.69		
AD3 – ^{11}C -PBR28	Right insula	36 -12 -9	4.53	<0.00001	363635
	Right middle frontal gyrus	21 10 35	4.24		
	Right fusiform gyrus	31 -9 -37	4.09		
	Left inferolateral remainder of parietal lobe	-34 -24 31	3.95		
	Left middle frontal gyrus	-25 37 -5	3.91		
	Right parahippocampus	26 -9 -34	3.89		
	Left posterior temporal lobe	-37 -36 0	3.85		
	Right inferolateral remainder of PL	41 -33 28	3.71		
	Left middle frontal gyrus	-21 44 3	3.66		
	Right posterior temporal lobe	48 -38 -15	3.66		
AD3 –^{18}F-AV1451					

	Left middle and inferior temporal gyrus	-62 -13 -27	5.41	<0.00001	294532
	Right superior parietal gyrus	2 -50 17	5.06		
	Left posterior temporal lobe	-57 -33 1	4.98		
	Right middle inferior gyrus	27 62 10	4.58		
	Left medial orbital gyrus	-6 61 -19	4.54		
	Left posterior cingulate cortex	-2 -40 25	4.51		
	Right middle and inferior temporal gyrus	56 -17 -22	4.77	0.005	51510
	Right posterior temporal lobe	55 -37 -3	4.14		
AD4 – ^{11}C - PBR28	Left anterior temporal lobe medial part	-26 1 -49	4.72	<0.00001	1000336
	Right inferolateral remainder of parietal lobe	32 -52 37	4.67		
	Right anterior temporal lobe lateral part	41 14 -37			
	Left posterior temporal lobe	-63 -42 -23	4.6		
	Right posterior cingulate cortex	2 -21 44	4.59		
	Right posterior temporal lobe	66 -46 -2	4.58		
	Left parahippocampus	-27 -14 -30	4,55		
	Left middle and inferior temporal gyrus	-37 -3 -42	4.53		
AD4 – ^{18}F-AV1451	Left middle and inferior temporal gyrus	-63 -14 -25	6.14	<0.00001	291873
	Left superior temporal gyrus posterior part	-64 -24 -6	5.44		

	Left posterior temporal lobe	-62 -37 -3	5.44		
	Right middle and inferior temporal gyrus	66 -20 -20	5.41	<0.00001	96228
	Right posterior temporal lobe	67 -34 -11	5.15		
	Right anterior temporal lobe lateral part	57 10 -25	4.58		
AD5 – ^{11}C -PBR28	Right hippocampus	31 -30 -6	4.91	0.034	15117
	Right middle and inferior temporal gyrus	43 -22 -12	2.64		
	Right parahippocampus	30 -24 -24	2.6		
	Right thalamus	18 -20 6	2.53		
	Right fusiform	35 -8 -30	2.5		
	Right posterior temporal lobe	50 -43 -12	2.46		
	Right anterior temporal lobe medial part	37 3 -33	2.43		
AD5 – ^{18}F-AV1451	Left middle and inferior temporal gyrus	-62 -3 -31	5.21	<0.00001	407247
	Left posterior cingulate cortex	-2 -41 27	5		
	Left lateral part of occipital lobe	-40 -69 -3	4.76		
	Right middle frontal gyrus	39 18 32	4.76		
	Left middle frontal gyrus	-24 30 38	4.72		
	Left medial orbital gyrus	-5 62 -21	4.55		
	Right middle and inferior temporal gyrus	56 -17 -22	4.52		
	Left posterior temporal lobe	-39 -63 16	4.49		
	Right middle frontal gyrus	39 18 32	4.76	<0.00001	38842
	Right superior frontal gyrus	20 23 44	4.43		

	Left inferior frontal gyrus	-40 32 12	3.09		
	Left superior frontal gyrus	-22 67 5	3.01		
	Left anterior orbital gyrus	-31 64 -6	2.74		
AD6 – ^{18}F-AV1451 only	Left lateral part of occipital lobe	-42 -67 -1	4.96	<0.00001	109095
	Left posterior temporal lobe	-39 -63 16	4.94		
	Left middle and inferior temporal gyrus	-63 -12 -31	4.24		
	Right posterior temporal lobe	45 -62 6	4.17		
	Corpus callosum	1 -28 17	3.99		
	Left inferolateral part of occipital lobe	Left inferolateral part of occipital lobe	-60 -27 20	3.95	
	Right middle and inferior temporal gyrus	50 -10 -45	3.9		
	Left lateral part of occipital lobe	-42 -67 -1	4.96	<0.00001	23218
	Left posterior temporal lobe	-47 -63 -10	4.08		
	Left inferolateral part of parietal lobe	-32 -49 28	5.19		
AD7 – ^{18}F-AV1451 Only	Left posterior temporal lobe		5.35	<0.00001	221890
	Left lateral part of occipital lobe		5.01		
	Right posterior temporal lobe		4.81		
AD8 ^{18}F-AV1451 Only	Right lingual gyrus	17 -74 3	4.79	0.002	59276
	Right posterior temporal	47 -65 -20	4.56		

	lobe				
	Right lateral part of occipital lobe	38 -73 -20	4.17		
	Right superior parietal gyrus	7 -55 16	3.74		
	Right cuneus	22 -64 17	3.7		
AD9 – ^{18}F-AV1451 Only	Left lateral part of occipital lobe	-33 -88 31	4.14	0.035	36365
	Left inferolateral part of parietal lobe	-49 -76 33	3.99		
	Left superior parietal gyrus	-43 -44 57	3.87		
AD10 – ^{18}F-AV1451 only	Left middle and inferior temporal gyrus		5.76	<0.00001	249033
	Let posterior temporal lobe		5.24		
	Left inferolateral part of parietal lobe		4.35		
	Left anterior temporal lobe medial part		4.24		
	Left superior temporal gyrus posterior part		4.2		
	Left inferolateral par of parietal lobe	-39 -63 47	3.66	0.007	48761
	Left superior parietal gyrus	-31 -60 55	3.55		
	Right superior parietal gyrus	28 -51 65	3.34		
	Right postcentral gyrus	52 -20 61	3.02		
	Right inferolateral remainder of parietal lobe	11 -40 73	2.92		
AV11-^{18}F-AV1451 Only	Right superior parietal gyrus	2 -50 17	6.33	<0.00001	768730

	Right posterior temporal lobe	50 -56 -24	6.11		
	Left posterior cingulate cortex	-2 -40 26	6.04		
	Left middle and inferior temporal gyrus	-63 -14 -25	5.96		
	Left posterior temporal lobe	-39 -63 16	5.86		
	Corpus callosum	1 -28 17	5.8		
	Left precentral gyrus	-25 -25 58	5.73		
	Right posterior cingulate cortex	5 -46 33	5.69		
AD12 – ^{18}F-AV1451 only	Right superior parietal gyrus	2 -50 17	6.49	<0.00001	871963
	Left precentral gyrus	-14 -54 -10	6.16		
	Left posterior cingulate cortex	-2 -40 26	6.09		
	Corpus callosum	1 -28 17	6.08		
	Right lingual gyrus	3 -66 0	6.03		
	Left middle and inferior temporal gyrus	-63 -14 -25	5.92		
	Left superior parietal gyrus	-1 -56 10	5.89		
	Left posterior temporal lobe	-39 -63 16	5.83		
AD13 – ^{18}F-AV1451 only	Left posterior temporal lobe	-55 -55 -23	5.54	<0.00001	271287
	Right lateral part of occipital lobe	37 -72 -19	5.46		
	Right posterior temporal lobe	50 -55 -24	5.22		
	Left middle and inferior temporal gyrus	-63 -13 -26	5.14		
	Left lateral part of occipital lobe	-40 -69 -4	5.06		
	Right lingual gyrus	2 -79 -8	5		

MCI 1– ^{18}F-AV1451 only	Left posterior temporal lobe	-54 -56 -24	4.69	0.007	9696
	Left lateral remainder of occipital lobe	-35 -73 20	4.42		
	Left middle and inferior temporal gyrus	-55 -23 -15	3.38		
MCI2 – ^{18}F-AV1451 only					
	Left middle frontal gyrus	-45 3 53	5.43	<0.00001	1171879
	Right middle frontal gyrus	35 43 31	5.4		
	Right superior frontal gyrus	17 38 52	5.26		
	Right inferolateral part of parietal lobe	43 -65 46	5.24		
	Left parahippocampus	-17 -8 -28	5.16		
	Left middle and inferior temporal gyrus	-41 -10 -45	5.09		
MCI3 – ^{18}F-AV1451 only	Right superior parietal gyrus	10 -61 27	5.13	0.008	48106
	Right middle and inferior temporal gyrus	62 -19 -34	4.19		
	Right parahippocampus	25 -22 18	3.9		
	Right fusiform gyrus	38 -14 -36	3.76		
	Right posterior temporal lobe	48 9 -46	3.58		
MCi4 – ^{18}F-AV1451 only	Right posterior temporal lobe	-55 -55 -23	5.7	<0.00001	314428
	Right superior parietal gyrus	9 -61 27	5.59		
	Left posterior temporal lobe	-59 -45 -27	5.58		
	Left superior temporal gyrus posterior part	-64 -29 5	5.37		
	Left middle and inferior temporal gyrus	-63 -13 -26	5.22		

	Left inferolateral part of parietal lobe	-56 -41 21	5.13		
	Left lateral part of occipital lobe	-43 -67 0	5.04		
MCI5 – ^{11}C - PBR28 only	Left anterior temporal lobe lateral part	-59 8 -24	3.81	<0.00001	5586
	Left middle and inferior temporal gyrus	-65 -5 -24	3.69	<0.00001	5586
MCI6 – ^{11}C - PBR28 only	Right fusiform gyrus	27 -4 -47	3.49	0.04	13309
	Brainstem	10 -35 -19	3.84	<0.00001	66332
	Left hippocampus	-20 -13 -16	3.82		
	Left posterior temporal lobe	-52 -37 -13	3,55		
	Left anterior temporal lobe medial part	-30 5 -30	3.5		
	Left parahippocampus	-24 -3 -38	3.47		
	Left posterior temporal lobe	13 -42 -3	3.17		
MCI7 – ^{11}C - PBR28	Right parahippocampus	25 -24 -17	3.07	0.007	19319
	Right superior temporal gyrus posterior part	41 -22 -8	3.01		
	Right fusiform gyrus	40 -18 -26	2.99		
	Right middle and inferior temporal gyrus	42 -13 -19	2.89		
MCI7 – ^{18}F-AV1451	Corpus callosum	5 -42 11	4.41		
	Right superior parietal gyrus	3 -51 16	4.36		
	Left posterior cingulate cortex	-2 -44 30	4		
	Right posterior cingulate cortex	4 -47 33	3.76		
	Right posterior cingulate	5 -4 45	4.15	<0.00001	2493

	cortex				
	Corpus callosum	7 1 29	3.97		
	Left posterior cingulate cortex	0 -19 47	3.71		
	Left anterior cingulate cortex	-6 -2 30	3.49		
	Left posterior temporal lobe	-58 -53 -3	4.03	<0.00001	3874
MCI8 -^{18}F-AV1451					
	Left middle and inferior temporal gyrus	-63 -14 -25	3.49	<0.00001	35715
	Right lateral part of occipital lobe	25 -79 38	3.41	<0.00001	72911
	Right inferolateral part of parietal lobe	62 -38 48	3.35		
	Left inferolateral part of parietal lobe	-48 -61 47	3.11	<0.00001	48056
	Left superior parietal gyrus	-33 -60 55	3.07		
AMY NEG1 – ^{11}C - PBR28	Right middle frontal gyrus	21 38 13	5.37	<0.00001	1398526
	Left postcentral gyrus	-12 -34 64	5.33		
	Right middle and inferior temporal gyrus	49 -10 -31	5.08		
AMY NEG 1 – ^{18}F-AV1451	Right postcentral gyrus	52 -20 61	3.73	0.002	61430
	Right inferolateral part of parietal lobe	61 -34 52	3.62		
	Left inferolateral part of parietal lobe	-50 -30 52	3.43		
	Left superior parietal gyrus	-31 -59 55	3.38		
	Left lateral part of occipital	-27 -98 10	3.38		

	lobe				
	Right middle frontal gyrus	42 13 59	3.33		
	Right superior frontal gyrus	22 19 64	3.26		
	Left postcentral gyrus	-42 -38 65	3.23		
AMY NEG 2 – ^{11}C - PBR28	Left straight gyrus	-7 13 -17	4.57	<0.00001	47101
	Right anterior temporal lobe lateral part	45 8 -38	4.46		
	Right fusiform gyrus	33 0 -30	3.68		
	Right middle and inferior temporal gyrus	47 -3 -35	3.66		
	Right posterior temporal lobe	50 -41 6	3.49		
	Right anterior temporal lobe medial part	39 0 -42	3.46		
	Right straight gyrus	6 10 -18	3.43		
	Left putamen	-21 7 -3	3.4		
	Left medial orbital gyrus	-11 13 -22	3.33		
	Left superior frontal gyrus	-12 37 42	3.61	<0.00001	24774
	Right posterior cingulate cortex	10 -18 34	3.39		
	Left precentral gyrus	-19 -18 56	3.19		
	Left anterior cingulate cortex	-3 18 28	3.12		
	Right superior frontal gyrus	10 27 38	3.09		
	Right anterior cingulate cortex	3 -2 35	3.08		
	Left posterior cingulate cortex	-7 -15 35	3.05		
	Left anterior cingulate cortex	-4 -1 42	2.96		
	Left superior parietal gyrus	-9 -48 59	2.95		

	Left superior parietal gyrus	-9 -48 59	2.95		
	Left superior frontal gyrus	-5 3 64	2.92		
AMY NEG 2 – ^{18}F-AV1451	Left anterior temporal lobe medial part	-23 12 -40	2.49	0.008	20633
AMY NEG 3 -^{11}C- PBR28	Right postcentral gyrus	34 -27 43	3.81	<0.00001	31528
	Right precentral gyrus	36 -23 49	3.72		
	Left superior parietal gyrus	-19 -39 68	3.65		
	Right superior parietal gyrus	31 -36 56	3.63		
	Right superior parietal gyrus	17 -48 56	3.54		
	Left inferolateral remainder of parietal lobe	-54 -28 47	3.52		
	Right superior frontal gyrus	9 -4 60	3.49		
	Left precentral gyrus	-34 -20 51	3.44		
	Right inferolateral remainder of parietal lobe	37 -65 40	3.4		
	Left postcentral gyrus	-18 -38 62	3.32		
	Right middle and inferior temporal gyrus	66 -23 -22	3.32	0.007	3730
	Right precentral gyrus	59 -1 9	2.86		
	Right superior temporal gyrus posterior part	65 1 0	2.8		
	Left lingual gyrus	-8 -86 -5	2.82	0.018	3262
	Right cuneus	5 -92 9	2.74		
	Left cuneus	-2 -91 -1	2.68		
	Right superior temporal gyrus posterior part	53 1 -13	3.47	0.002	4545
	Right superior temporal gyrus anterior part	48 18 -22	3.45		
	Right middle frontal gyrus	23 51 -4	3.41		

	Right anterior temporal lobe medial part	38 10 -25	3.13		
	Right inferior frontal gyrus	48 36 -9	2.89		
AMY NEG 3 - ^{18}F-AV1451	Right superior frontal gyrus	22 20 63	4.91	<0.00001	132871
	Left precentral gyrus	-25 -25 58	4.74		
	Right middle frontal gyrus	54 19 41	4.69		
	Left superior frontal gurus	-13 28 60	4.37		
	Left middle frontal gyrus	-28 2 65	4.34		
	Right precentral gyrus	59 7 40	4.29		
AMY NEG 4 – ^{11}C - PBR28	Right middle and inferior temporal gyrus	44 -31 -12	4.07	<0.00001	30488
	Right posterior temporal lobe	44 -35 -15	3.12		
AMY NEG 5 – ^{11}C - PBR28	Left insula	-33 15 6	4.77	<0.00001	909967
	Right middle frontal gyrus	21 38 -8	4.68		
AMY NEG 6 – ^{18}F-AV1451	Right lingual gyrus	2 -81 -7	4.52	<0.00001	279556
	Left precentral gyrus	-25 -25 58	4.32		
	Right superior frontal gyrus	24 20 63	4.25		
	Right middle frontal gyrus	43 13 54	4.06		
	Right precentral gyrus	69 -5 25	3.9		
	Left postcentral gyrus	-26 -29 61	3.89		
	Left superior parietal gyrus	-1 -52 64	3.86		
	Left posterior temporal lobe	-60 -53 -4	3.85		
	Right inferolateral part of parietal lobe	65 -43 27	3.79		
	Right superior parietal	18 -55 58	3.77		

gyrus

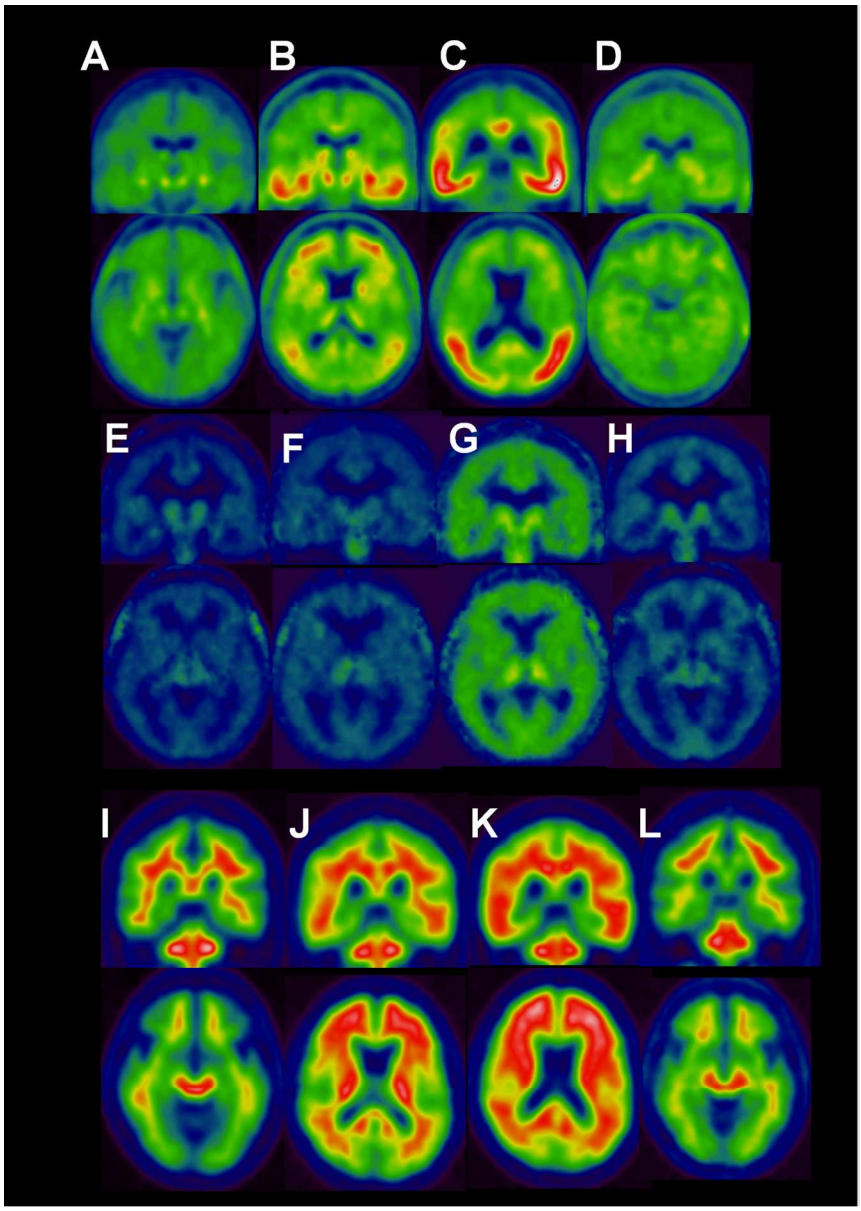

150x210mm (300 x 300 DPI)

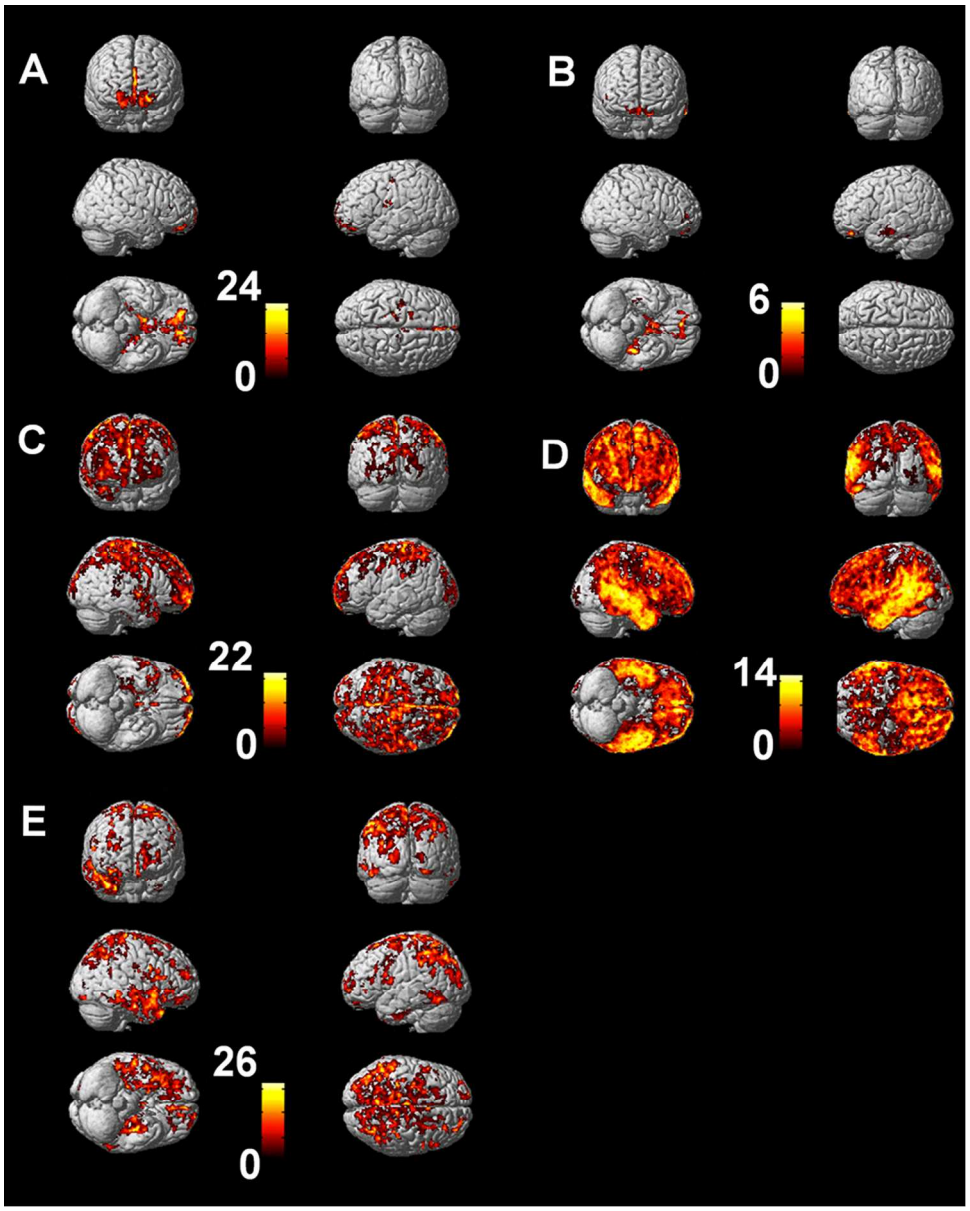

203x254mm (300 x 300 DPI)

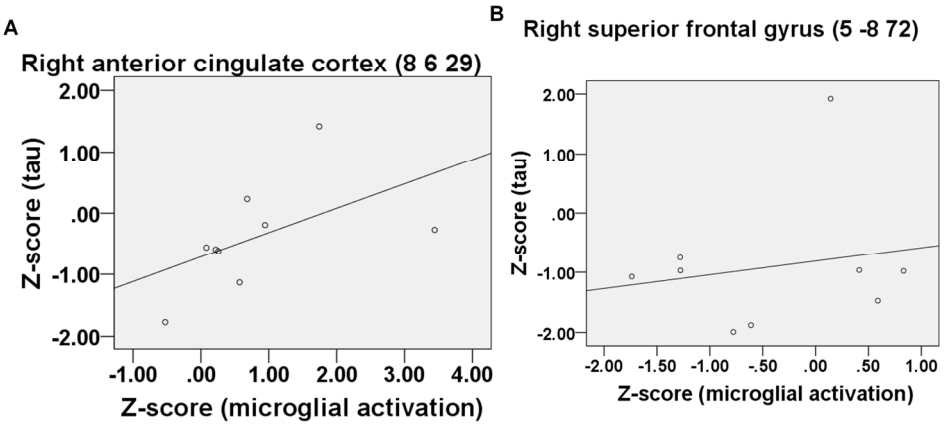

184x104mm (300 x 300 DPI)

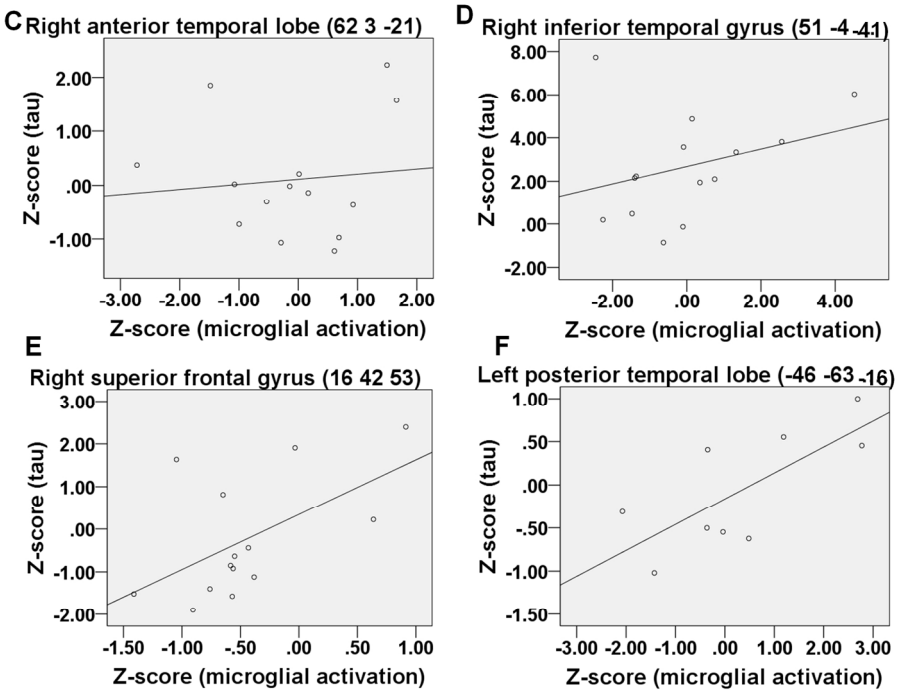

184x132mm (300 x 300 DPI)

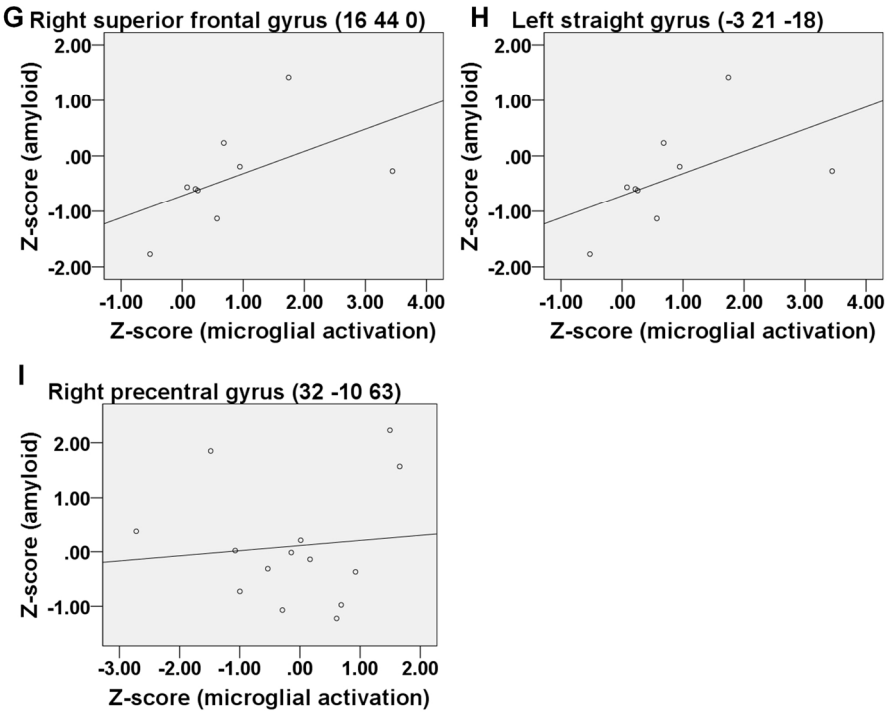

184x137mm (300 x 300 DPI)

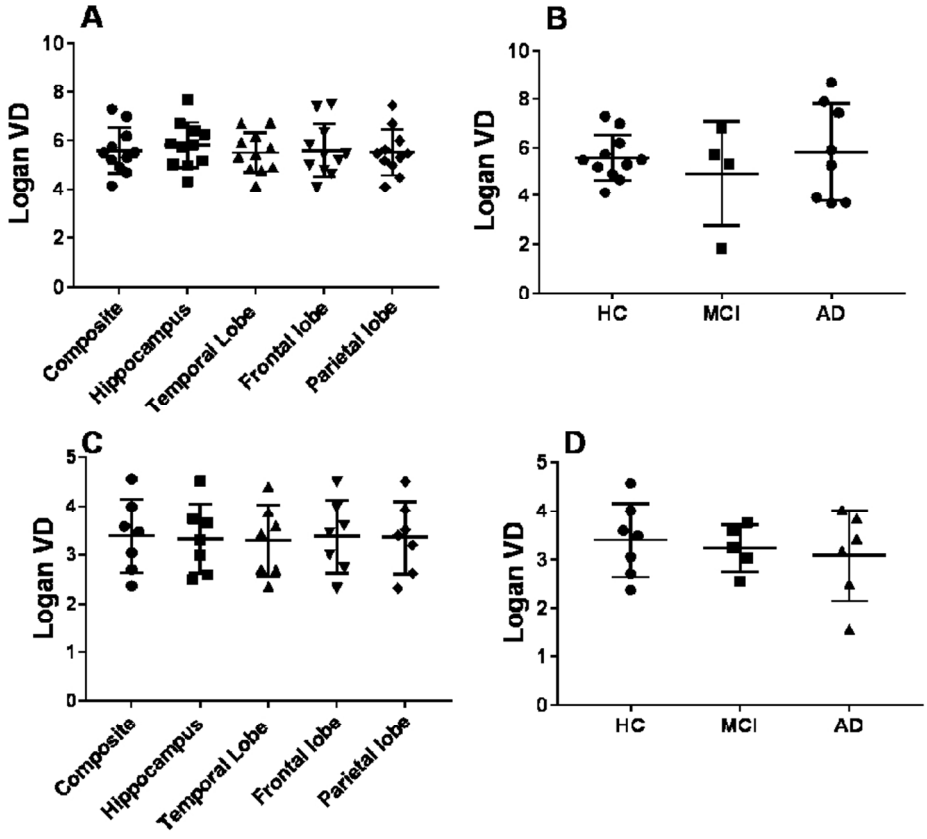

90x76mm (300 x 300 DPI)